11

High-Voltage (Underground) Cables

In spite of their economic advantage and wide application, overhead transmission lines suffer two inherent drawbacks:

1. Their exposure to atmospheric conditions that may considerably hamper their performance and therefore has to be taken into account in their design.
2. Their rather large insulation clearances, which result in line towers of considerable sizes, require large corridors for the entire length of the line.

High-voltage cables provide answers to these drawbacks by providing

- A contained insulating environment that ensures stable operating conditions and protects the insulation against atmospheric conditions
- Compact dimensions that compare advantageously with overhead lines, even at high voltages

This comes, however, at a substantially higher price, an order of magnitude compared to that of the overhead lines, and has also their own drawbacks. As a result, the use of high-voltage cables is limited to particular applications when the constraints, either natural (water crossings, mountains, etc.) or social (restrained space, city environment, etc.), exclude the application of overhead lines.

11.1 Development of High-Voltage Cables

The interest in high-voltage cables dated back to the beginning of the twentieth century—the first high-voltage cable was developed by S. de Ferranti in 1891—and contributed to sustain their constant evolution towards higher voltages and power transmission capacities. Unlike overhead lines, the development of high-voltage cables has a wide diversification depending on the development of new insulating materials and competition between different cable technologies. Actually, high-voltage cables exist in one of the three categories, identified by the mode of insulation: impregnated paper–oil, solid (extruded), and compressed gas–epoxy.

11.1.1 Paper–Oil-Insulated Cables (Couderc, 1987)

Introduced in 1891 by S. de Ferranti, the insulation by paper impregnated with ozokerite, a by-product of the candle wax, offers an elegant solution to the problem of cable insulation and is precursor to the paper–oil insulation used in modern cables. The paper–oil insulation suffered, however, of partial discharges (PDs) developing in the voids formed between the layers of paper tapes, which caused premature failures of the initial cables using this type of insulation. For many years, the utilization of these cables was limited to voltages below 30–35 kV. The use of pressurization with nitrogen at pressures of 1.1–1.38 MPa (160–200 psi) partly solved the PD problem and gave rise to the pressurized-gas paper-impregnated cable developed in 1943. This solution reached its full potential only with the introduction of lapped paper for the flexibility of the cable and pressurized fluid oil, introduced by Emmanuelli in 1926, to improve the dielectric performance, namely, by the elimination of voids containing air (or gas), constituting sites of PDs responsible for the slow degradation of the impregnated paper insulation. Figure 11.1 gives an overview of the development of cables with pressurized insulation made of lapped impregnated paper. The bold characters indicate the current types of cable.

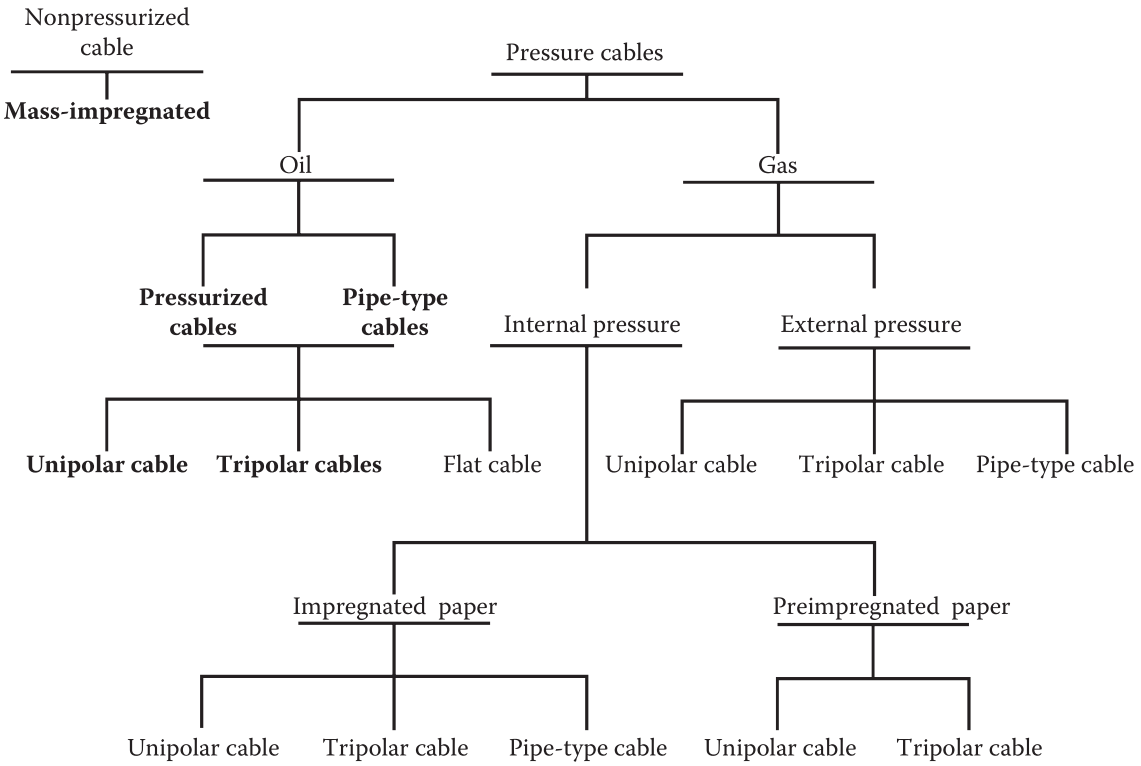

FIGURE 11.1 Cables with pressurized lapped paper insulation. (Couderc, D. Revue de l'État des Technologies des Câbles de Transport a Très Haute tension en Courant Alternatif et Continu, IREQ report, IREQ, Varennes QC, Canada, November 1987.)

11.1.1.1 Pressurized Oil-Filled Paper-Impregnated Cables

Pressurized oil-filled paper-impregnated cables are presently the most widely used because of their proven reliability, their availability over a wide range of voltages and power transmission capability, and above all, the long experience of manufacturers and users with this type of cable. Two main categories of paper–oil insulation exist for ac cables: self-contained oil-filled (SCOF) and high-pressure oil-filled (HPOF).

Self-contained oil-filled cable: In SCOF cables with internal oil pressure (Figure 11.2), the hollow conductor is filled with pressurized oil, typically at 450 kPa, which diffuses from the center to the insulation periphery. The latter comprises several layers of paper tapes of high purity, with a thickness varying from

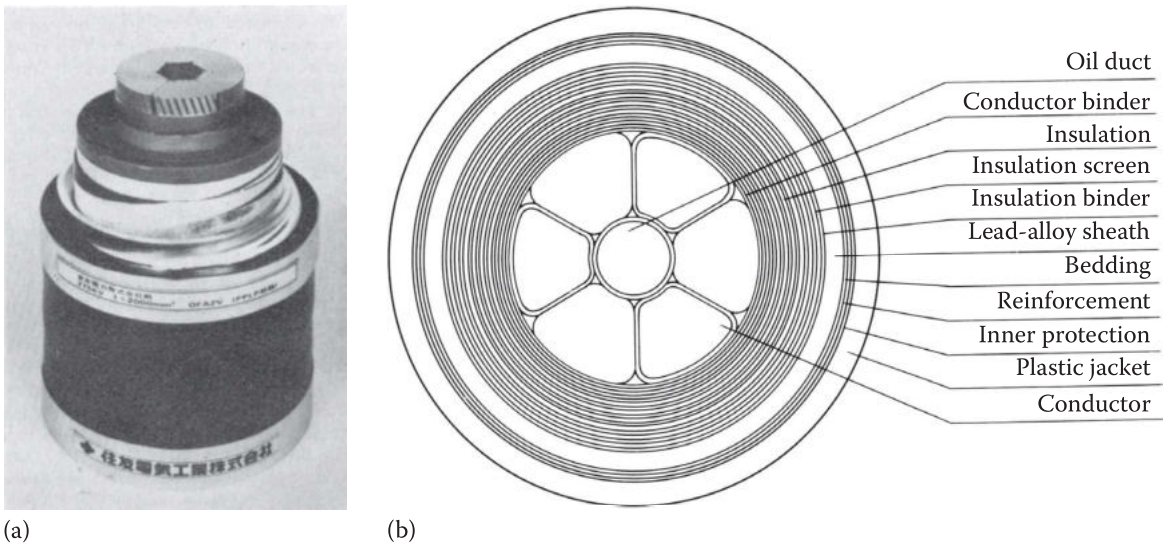

(a) (b)

FIGURE 11.2 Single-phase oil-filled cable. (a) SCOF cable; (b) schematic representation. (From Kubo, H. et al., *IEEE Trans.*, PAS-101(12), 4472, 1982.)

25 to 250 μm and width that varies with the distance from the conductor. An outer metal sheath maintains the oil pressure in the cable and protects the insulation against contamination. The SCOF cable is predominantly used in high-voltage cable circuits worldwide, at voltages up to 500 kV ac and ±500 kV dc.

Impregnation of paper insulation is made by filling the central channel with oil of low viscosity, allowing the oil to diffuse across the cable insulation during thermal cycles. This is done by connecting the central channel to sealed underground reservoirs with expansion bellows to compensate the variations in the oil volume during the thermal cycles of the cable while maintaining a constant pressure in the oil. The majority of existing cables use mineral oil as impregnating fluid. The introduction of synthetic oils has gradually changed the situation in favor of the latter as impregnating oil in paper–oil cables. In the 1960s, it was dodecylbenzene (DDB); more recently, *alkylate* oils like the decylbenzene (DB) and the *nonylbenzene* (NB) are becoming popular due to their low viscosity and good capacity to absorb water vapor liberated during aging of cellulose fibers. SCOF cables are widely used in Europe where cable circuits operate at voltages of 400 and 500 kV. In North America, 525 kV is the highest voltage reached by SCOF cables (Bellport, 1970). Sections of 750 kV cables have been successfully tested. The maximum admissible transmission power can reach, with forced cooling, the level of 10,000 MVA at 1,100 kV ac (Farnetti et al., 1984b).

High pressure oil-filled cables: In HPOF cables with external oil pressure, three or more paper-taped cables are placed inside a rigid steel pipe maintained under oil pressure (Figure 11.3). Each of the elementary cables is of similar structure to those in SCOF cables, except for the viscous impregnating fluid. The insulation, also of taped cellulose paper, is covered with a metal screen, which fixes the potential at the periphery of the cable, while protecting the insulation against humidity during storage and cable laying.

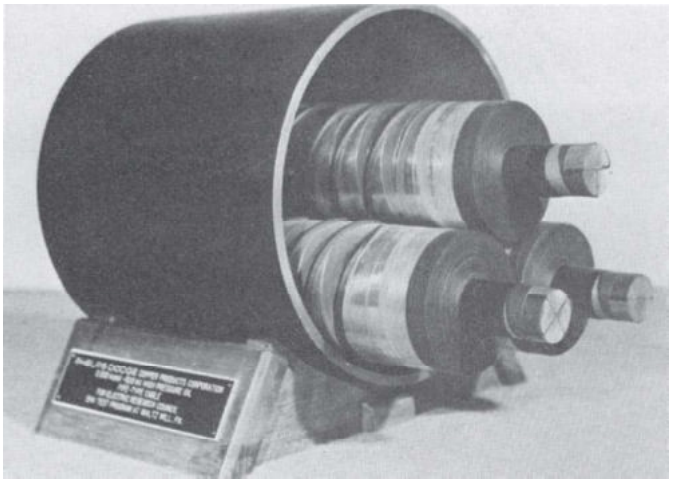

(a)

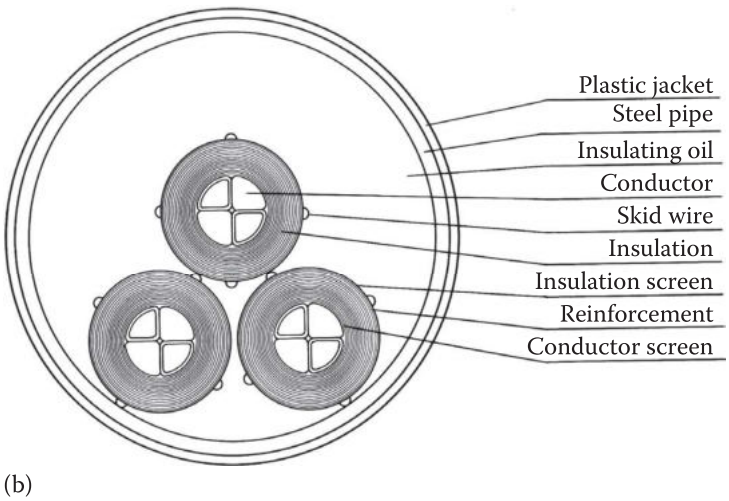

(b)

FIGURE 11.3 Three-phase oil-filled cable. (a) HPOF pipe-type paper–oil cables; (b) schematic representation. (From McKean, A.L. et al., IEEE Trans., PAS-90(1), 224, 1971.)

Maintaining an external oil pressure does not require a central channel for the oil circulation. The cables and their paper insulation are impregnated in factory. To facilitate cable laying into the pipe, sliding wires with D-shape cross section, of metal or high-density polyethylene (PE), are wound in long pace around each elementary cable. HPOF cables are widely used in North America up to voltages of 345 kV. Cables of 550 kV are available, and tests have been made on sections of 765 kV (Allam et al., 1986).

In spite of the various options used by different cable manufacturers, paper–oil insulation has the following typical characteristics: a relative permittivity of 3.5, a loss factor between 0.3% and 0.5%, and a thermal resistivity of about 500 m°C/W. The oil pressure is between 520 and 620 kPa (75–90 psi) for SCOF cables and about 1.38 MPa (200 psi) in pipe-type cables. This difference in the oil pressure gives pipe-type cables a slightly better dielectric performance, of around 10%, as compared to SCOF cables.

The principal limitation of impregnated paper–oil insulation resides in their high dielectric losses, which tends to favor thermal breakdown. Thermal breakdown can occur even if the high-voltage cable does not carry any current, and the sheath is at ambient temperature, making their utilization at voltages above 800 kV ac almost impossible. This, even if a prototype 1100 kV ac cable by Pirelli, has successfully passed a long-duration demonstration program by *ENEL*. The 1100 kV ac cable is, in fact, a 750 kV ac cable for which the internal oil pressure was increased to 1.3 MPa to enhance the operating gradient to 30 kV/mm. The length of the test cable, at Suvereto, was about 200 m, comprising joints and terminations as well as an external cooling system (Farnetti et al., 1984).

Practical experience shows that paper–oil insulation develops permanent deformations at temperatures higher than 120°C, and it is not recommended to operate the cable at 100°C, corresponding to a temperature difference of about 80°C between the central conductor and the sheath. The current practice favors a range of operating temperature of 70°C–90°C for paper–oil-insulated cables.

11.1.1.2 Mass-Impregnated Cables

Mass-impregnated cables use an impregnating material, which is viscous at ambient temperature and gives the impression of a solid insulation when the cable is dissected. Under load condition, where the cable heats up, the impregnating material liquefies and diffuses into the paper insulation. However, the dilatation of the materials sustains a temporary pressurization, which disappears when the cable cools down, producing gaseous voids in the butt gaps. The existence of gas voids, which becomes PD sites, is a major handicap in ac voltage application, limiting its use to voltages below 63 kV ac. The effect of gas voids is somewhat less severe in dc voltage where the utilization of mass-impregnated cable extends up to voltages of 400 kV dc and is under consideration for the level of 500 kV dc. They are presently the only candidate for long submarine crossings where the cables are subjected to considerable hydrostatic pressures and a serious competitor to internal oil pressure cables, even at high-voltage levels.

11.1.2 Extruded Insulation Cables

The first application of solid insulation in high-voltage cables dates back to 1888 with the use of vulcanized rubber. The low dielectric strength of the rubber however limits its use to low-voltage cables. The copolymerization of synthetic rubber with ethylene and propylene improves the dielectric performance of rubber while keeping good flexibility and high deformation temperature up to 135°C. The use of EPR is limited to voltages below 100 kV.

The principal breakthrough in solid insulation cables was obtained by the use of polymers PE and XLPE. Practical experience shows that the extrusion of polymers in thick layers is delicate to ensure that the insulation is free of voids and solid impurities, which can initiate PDs, particularly damaging to both PE and XLPE. The development of extruded cables was largely dependent on progress realized in the techniques of extrusion and quality control processes. From a nominal voltage of 25 kV in the 1960, extruded cables have reached the level of 225 kV ac and then 400 kV ac in 1986 with the commissioning of an EDF cable system using natural PE of SILEC (Jocteur et al., 1986).

Figure 11.4 illustrates the typical construction of the solid insulation cable. The central copper conductor has a cross section chosen for the required power transmission capacity. The PE insulation is coextruded in sandwich between two layers of semiconducting (carbon-filled) PE to ensure good adhesion between the different layers and, thus, minimize the risk of separation of the layers during thermal

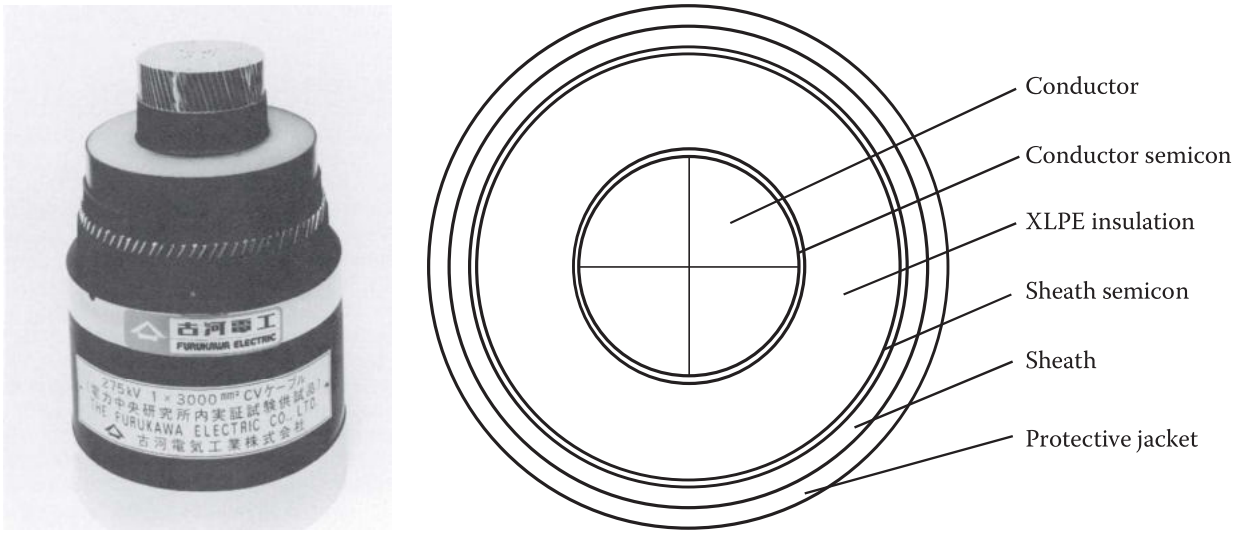

(a) (b)

FIGURE 11.4 Polymer-insulated cable. (a) XLPE-insulated cable; (b) schematic representation. (From Fukuda, T., *IEEE Electric. Insul. Mag.*, 4(6), 15, 1988.)

cycles. A lead sheath covers the insulation to protect against the water infiltration. Finally, a PVC protective jacket is extruded on the lead sheath to protect against corrosion.

Cross-linked polyethylene (XLPE), more economical than PE with better mechanical properties and a higher operating temperature (90°C compared to 65°C–70°C for PE), is widely used in low and medium voltages. Improved methods of manufacture have provided a high homogeneity of the insulating material, minimizing migration of impurities and simplicity of manufacture that allowed XLPE cable to reach the level of 500 kV ac in the 1990's with the commissioning of 500 kV cable system by Tokyo Electric Power Co.

11.1.3 Cables with Gas Insulation

11.1.3.1 Pressurized-Gas Cables

The first application of compressed gas insulation was introduced to minimize the effect of voids on the dielectric strength of the paper–oil insulation. The individual cables with paper–oil insulation are placed in an external envelope capable to sustain a high gas pressure, usually nitrogen at a pressure of 1100–1380 kPa (160–200 psi). Pressurizing the paper–oil insulation reduces the size and increases the inception voltage of PDs in the gas voids, thus improves the dielectric performance of the insulation. These cables are used mainly in submarine crossings; two important achievements are as follows: the three-phase link of British Columbia to Vancouver Island using unipolar 138 kV cables, with a hollow conductor for the gas to propagate over long distance. The other is the 48 km crossing at the strait of Cook, in New Zealand, with a 600 MW, 250 kV dc link.

The rapid development of the SCOF and pipe-type cables has made pressurized-gas cables less appropriate for ac voltage, while for dc voltage, they are replaced by nonpressurized mass-impregnated cables. Obviously, it is much more difficult to maintain a gas pressure of 1400 kPa than an equivalent oil pressure. This situation also favors the development of the rigid gas-insulated cables, also known as gas-insulated lines (GIL), because of the rigid structure of the cable.

11.1.3.2 Rigid Gas-Insulated Cables (Lines)

Gas insulation, because of its less competitive dielectric strength, has traditionally been neglected by the cable industry, for which compactness and flexibility are the key parameters. In effect, even with a clearance distance of 1/10 of air insulation, SF_6-insulated cables operating at 4–5 atm abs are still several times larger than conventional paper–oil-insulated cables of the same voltage rating. Instead, it is the combination of the good arc-quenching propriety of SF_6, its adequate insulating performances, and

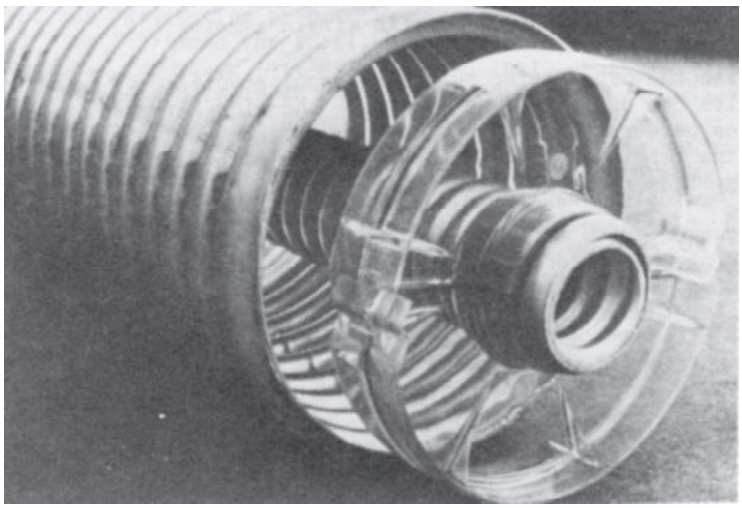

(a)

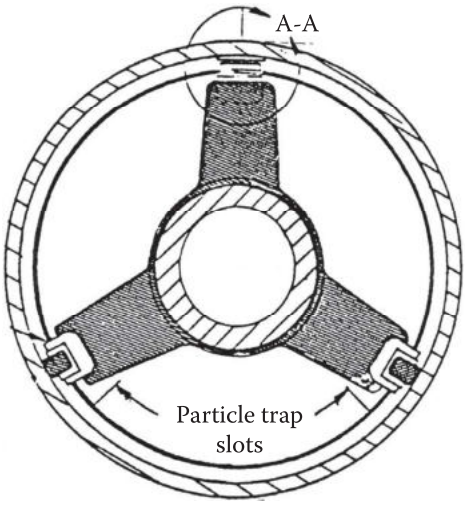

(b)

FIGURE 11.5 Gas-insulated cables. (a) Flexible SF_6-insulated cable; (b) rigid cable with tripod spacer. (From Cookson A.H., *IEEE Trans. Electr. Insul.*, EI-20, 859, 1985.)

above all, its nonflammability, which promotes development of SF_6-insulated switchgear, at first as single pieces of equipment and then their integration into a full-scale substation.

It is only when the development of gas-insulated stations (GISs) has reached 345 kV that gas-insulated cables, with their high power transmission capacity with critical length comparable to that of overhead lines and hence its designation as GIL and low dielectric losses, gain their competitive edge over conventional cables. The combination of compact GIS with long gas-insulated cables provides an elegant solution to transmit the output power of underground generating stations to overhead lines, which has been used by several utilities (Cookson, 1985). It reached 420 kV in Europe (Wehr station) and 500 kV ac level in Japan and in North America: the underground link in the Cascades (United States) in 1975 (De Maris, 1975) and the Mica project of BC Hydro in 1976. Short lengths of 800 kV ac cables are operating in the Guri Central in Venezuela since 1984.

The design of rigid gas-insulated cables is relatively simple: insulating spacers maintain the metal conductors in place within a cylindrical tube, containing compressed SF_6, at 0.3–0.5 MPa. To make gas-insulated cables more competitive, flexible and semiflexible cables have been evaluated. The conductor is composed of aluminum strands, the outer sheath is of corrugated aluminum, and spacers, in greater number, are molded from more economic plastic shown in Figure 11.5. A short length of a 1200 kV ac flexible gas-insulated cable has been tested by EPRI in the 1990s (Bolin et al., 1982; Gnadt and Walldorf, 1995).

11.1.4 Future Trends in High-Voltage Cables

With the current trend for high-voltage power transmission systems to 1200 kV ac in Russia and China and ±800 kV dc in China, development of high-voltage cables will turn to improve the current technology to make them more economical to produce and operate, namely, to increase the power transmission capability and to reduce dielectric losses.

11.1.4.1 Forced Cooling

Forced cooling can almost double the power transmission capacity of cable circuits. Table 11.1 illustrates, in effect, the potential ac power transmission capacity reached by high-voltage cables with appropriate forced cooling technologies (Morello et al., 1985). The adaptation to forced cooling requires the installation of a channel for the circulation of the cooling liquid and stations of heat exchange at regular intervals, a few kilometers, along the cable circuit. Early installations of forced cooling used water circulating in conduits installed in parallel to the cables. The current trend is to circulate the cooling fluid in a channel within the conductor. Oil-filled cables, both SCOF and HPOF, are easily adapted to forced cooling with the insulating oil serving at the same time as cooling liquid. Forced cooling of solid XLPE insulation cable with water circulating in a central channel was evaluated in Japan in 1987 (Kobayashi et al., 1985; Ogawa et al., 1989).

TABLE 11.1

Power Transmission Capacity (in MVA) of HVAC Cables with Forced Cooling

Cable	Cooling	Length, km	110 kV	220 kV	400 kV	800 kV	1000 kV
SCOF	Ext./Water	0.5	1,700	3,500	5,000	5,000	
SCOF	Ext./Water	2.5	800	1,500	2,200[a]	2,200	
SCOF	Surf./Water	0.5	2,300	4,500	6,500	6,500	4,500[a]
SCOF	Surf./Water	2.5	1,000	1,900	2,900	2,900	2,000
SCOF	Cond./Oil	0.5	3,500	7,000	10,000	10,000	6
SCOF	Cond./Oil	2.5	1,000	2,000	3,000[a]	3,000	2,600
SCOF	Cond./Water	0.5	4,700	10,000	10,000	10,000	10,000[a]
SCOF	Cond./Water	2.5	1,400[a]	3,000	3,000	3,000	3,000
HPOF	Surf./Oil	0.5	1,200	2,400	3,200	4,200	10,000
HPOF	Surf./Oil	2.5	550	1,100	1,500[a]	2,000[a]	3,000
PE	Cond./Water	0.5	2,500	5,000			
PE	Cond./Water	2.5	750	1,500[a]			
XLPE	Cond./Water	0.25			1,500[b]		
SF_6	N/A		1,400	3,000	7,000[a]	13,000	18,000[a]

Source: Morello et al. 1985.

[a] Values obtained by measurement or by calculation.

[b] Results from long-term tests on 275 kV cable.

The use of forced cooling may cause certain problems related to the overheating of cable joints, their insulation built in site, that are generally thicker and dissipate the generated heat less efficiently.

11.1.4.2 Synthetic Paper and Tape

The main limitation of oil-impregnated paper cables resides in their high dielectric losses, which makes their use at voltages higher than 800 kV ac almost impossible. Several attempts to reduce the dielectric losses have been made, using synthetic tapes, polypropylene films, and composite films formed of a polypropylene film in sandwich between two cellulose tapes. Table 11.2 gives the main characteristics of these synthetic insulations, considered for use in high-voltage cables. Among many candidates investigated, the polypropylene paper laminate (PPL) composed of a polypropylene film inserted between two *kraft* paper tape layers, the total thickness of the PPL tape being comparable to that of an equivalent paper tape, stands out as the most promising. The PPL represents a good compromise between the required mechanical qualities of the cellulose paper and the excellent electric properties of polypropylene. It can be seen from Table 11.2 that the PPL is superior concerning the dielectric constant, the losses, and the dielectric strength in ac and impulse voltages. PPL–oil-insulated cables are in service in Japan at 275 kV

TABLE 11.2

Characteristics of Synthetic Lapped Insulation

Parameters	Units	PPL	Polypropylene	Kraft
Thickness	mm	100	125	100
Resistance to traction	MN/m^2	76	22–35	110
Elongation at rupture	%	2.7	4–6	3.1
Density		0.9	0.75	0.95
Relative dielectric constant		2.7	2.2	3.4
Loss factor tanδ		8×10^{-4}	3×10^{-4}	2.3×10^{-3}
Positive impulse	kV/mm	190		135
Negative impulse		150		135
AC dielectric strength	kV_{rms}/mm	55	60	50
Permeability to air	Gurley-s	3,000	15,000	

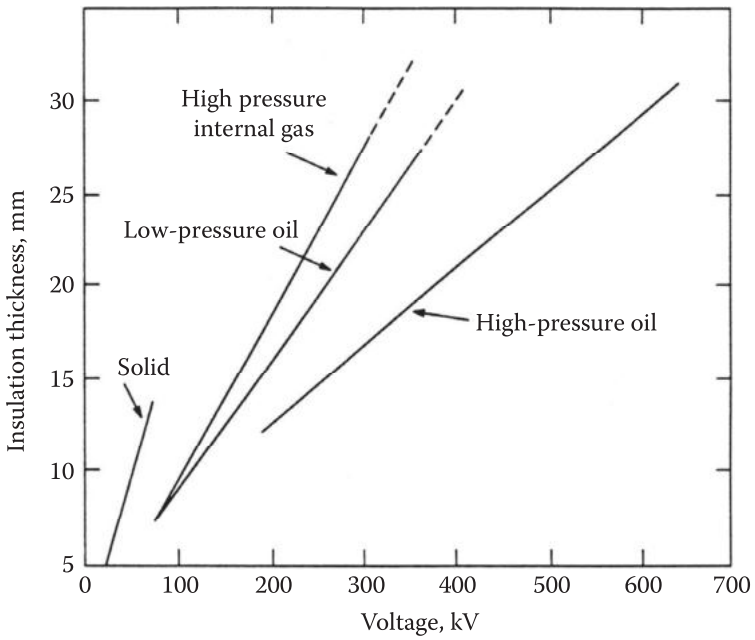

FIGURE 11.6 Influence of the pressure on the insulation thickness of different types of ac cables. (From Couderc, D. Revue de l'État des Technologies des Câbles de Transport a Très Haute tension en Courant Alternatif et Continu, IREQ report, IREQ, Varennes QC, Canada, November 1987.)

since 1980 and 525 kV since 1985. In the United States, a pipe-type PPL–oil-insulated cable of 345 kV is in service since 1985, while a prototype of 765 kV is under evaluation by Phelps Dodge (Cablec).

11.1.4.3 Pressure

Figure 11.6 illustrates the influence of pressure on dielectric strength and thickness of the insulation of different types of cables. It can be seen that pressurized-gas cables cannot compete with oil-filled cables due to the lower dielectric strength of gases. The higher the internal pressure of the cable, the higher the operating gradient can be. This gradient is 10–12 kV/mm for low-oil-pressure cables (≤500 kPa). It increases to 15–28 kV/mm for higher oil pressures up to 1500 kPa in cables of 400 kV and higher. As for the nonpressurized mass-impregnated cable, the presence of gas voids as PD sites limits its use to dc voltages only, particularly in applications requiring the immersion of great lengths of cables, when they are subjected to considerable hydrostatic pressures.

11.1.4.4 Compressed SF_6-Insulated Cable

Penalized by its relatively large size, compressed SF_6-insulated cables offer an alternative to transmission of large bulk power at high voltage, above 500 kV ac, where the dielectric losses become a serious drawback to oil-filled cables. The low losses of SF_6-insulated cables allow their use over long distances up to several hundreds of kilometers without compensation. Their large size also minimizes the need of forced cooling and allows operating at close to their natural power transmission capacity.

11.2 High-Voltage AC Cables and Accessories

Electric field distribution: High-voltage ac cables, those operating at EHV levels in particular, are single-core, coaxial configuration. The field distribution in the cable insulation is

$$E(r) = \frac{U}{\ln(b/a)} \frac{1}{r} \tag{11.1}$$

where a and b are the radii of the center conductor and envelope.

The following expressions are for the field at the central conductor E_0 and at the outer sheath E_s:

$$E_0 = \frac{U}{\ln(b/a)}\frac{1}{a} \tag{11.2}$$

$$E_s = \frac{U}{\ln(b/a)}\frac{1}{b} \tag{11.3}$$

11.2.1 Cable Parameters

A number of parameters characterize ac cable in coaxial configuration, relating their physical dimensions to their electrical parameters as follows:

The cable capacitance C per unit length is

$$C = 2\pi\varepsilon\frac{1}{\ln(b/a)} \quad \text{F/m} \tag{11.4}$$

The cable inductance L per unit length is

$$L = \frac{\mu}{2\pi}\ln\frac{b}{a} \quad \text{H/m} \tag{11.5}$$

The propagation velocity of electromagnetic wave is

$$v = \frac{1}{\sqrt{LC}} = \sqrt{\frac{1}{\mu\varepsilon}} \quad \text{m/s} \tag{11.6}$$

Characteristic impedance Z_0 is

$$Z_0 = \sqrt{\frac{L}{C}}\ \Omega \tag{11.7}$$

Natural transmission capacity P_p is

$$P_p = \frac{U_p^{\,2}}{Z_0}\ \text{MVA} \tag{11.8}$$

where

P_p is the natural transmission capacity per phase of the line (MVA)
U_p is the nominal phase-to-ground voltage (kV)
ε is the permeability
μ is the susceptibility

Because of the excellent dielectric performance of cable insulation systems, the insulation thickness is often less than the optimal value for a minimum gradient at the central conductor. The capacitance is in the range of a few tens of pF/m, and the cable characteristic impedance a few tens of Ohms, compared to a value of a few hundreds of Ohms for overhead lines. As a result, high-voltage cables have a natural power transmission capacity many times higher than an overhead line operating at the same voltage.

Effective power transmission capacity P_l *and critical length* L_l: For overhead lines, the natural transmission capacity is a determining parameter; it is much less so for high-voltage cables, where the high dielectric losses combined with the low efficiency of heat transfer of the soil limit the load current to an effective value I_L. Except for the case of unburied gas-insulated cables, power transmission of

high-voltage cables is reduced considerably below their natural transmission capacity defined from Equation 11.7, according to

$$P_L = U_p I_L \tag{11.9}$$

and the critical length to

$$L_c = \frac{I_L}{\omega C U_p} \tag{11.10}$$

SF_6-insulated cables, with their low permittivity and high ampacity, have longer critical lengths, reaching several hundreds of kilometers. Solid polymer-insulated cables follow with critical lengths in the range of a few hundreds of kilometers. The impregnated paper–oil-insulated cables, penalized by a high permittivity and notable dielectric losses, have a critical length of a few tens of kilometers only. However, except for submarine link, which can reach several tens of kilometers, cable circuits are usually part of a larger overhead line transmission system, and their lengths are kept to minimum, in the range of a few kilometers.

11.2.2 Dimensioning of the Conductor

In spite of the wide variety of insulating materials and insulation systems available, the dimensioning of high-voltage cables follows a few general rules presented in the following for the selection of the conductor and cable insulation.

Table 11.3 compares typical characteristics of high-voltage cables. Although the natural load current I_n given by

$$I_n = \frac{P_n}{U_n} = \frac{U_n}{Z_0} \tag{11.11}$$

can be high, it may not correspond to the maximum admissible current in a high-voltage cable, determined by the limit temperature at which the cable can operate without danger. This limit temperature is in the range between 70°C and 85°C for most cables and provides an adequate safety margin below the temperatures causing thermal instability to the insulation, in the range of 100°C–135°C. For buried cables, a second limit temperature exists and corresponds to the local temperature of the soil, which must be maintained at a safe level, of about 85°C, to avoid drying of the soil and thermal runaway, which might follow.

It should be noted that often, a cable circuit is only a part of a transmission system largely composed of overhead lines, which determine both the load current and the nominal voltage for the cable circuit. Dimensioning the cable conductor consists of minimizing the total losses, taking into account the available heat dissipation system. The designing parameters are the resistive heat generated by the conductor, the dielectric losses in the cable insulation and sheath, and the characteristic of the thermal dissipation system. Since the insulation thickness is determined by the electrical stresses to the cable, its dielectric losses are a function of the conductor dimension. An iterative process results in which the cable conductor is varied to adjust the generated resistive heat to limit the maximum temperature at the conductor below the selected safe value. These aspects are discussed in the following.

Conductor design: To provide the required flexibility, the conductor, copper or aluminum, is built up from small metal strands. The conductor for SCOF cables is hollow to make up a channel for the circulation of the impregnating oil. Conductors of small section are made of several layers of copper or aluminum wires around a steel spiral to form the oil channel. Conductors of large section, above 800 mm^2 (1580 kcmil), use one of the two designs, *Conci* or *Milliken*.

The *Conci* design shown in Figure 11.7 uses strands of trapezoidal section, imbricated one to another to form a self-supporting arch. The conductor has several layers, three in the case of 800 mm^2 conductor, with the strands spiraled in opposite directions in two adjacent layers to provide better mechanical behavior. The *Conci* conductor provides a high degree of compactness, of about 98%, and forms naturally a channel for the circulation of the impregnating oil of SCOF cables. Hollow conductors are also

TABLE 11.3

Typical Characteristics of High-Voltage Cables

	Units	SCOF/HPOF	Polymer	SF_6 Insulation
Conductor				
Section maximum	mm^2	3040/1270	2500	
Radius	cm	3.5/2.5	3	10–25
Thickness	mm			12.7
Nominal field				
AC	kV_{rms}/mm	150/170		100
DC	kV/mm	270/310		150
Temperature	C	70–90	70	70–90
Ampacity	kA		0.6–1.5	4
Insulation				
Thickness	cm	0.5–2.5	2.5	10–25
AC dielectric strength	kV_{rms}/mm	50–55	16–25	
Impulse dielectric strength	kV/mm	95–135	50–75	
Relative dielectric constant		3.5	2.5	1
Loss factor		2.5×10^{-3}	3×10^{-4}	
Loss factor		8.8×10^{-3}	0.7×10^{-3}	
Thermal resistivity	m C/W	500	350	
Deformation temperature	C	120	90–135	105–135
Sheath				
Material		Lead, aluminum		Aluminum
Thickness	mm	6		5–10
Cable Parameters				
Capacitance	pF/m	200–500	150–250	55
Critical length	km	50–90	70–150	500
Soil Characteristics				
Thermal conductivity	W/m C	1–2.5		
Thermal resistivity	m C/W	100		

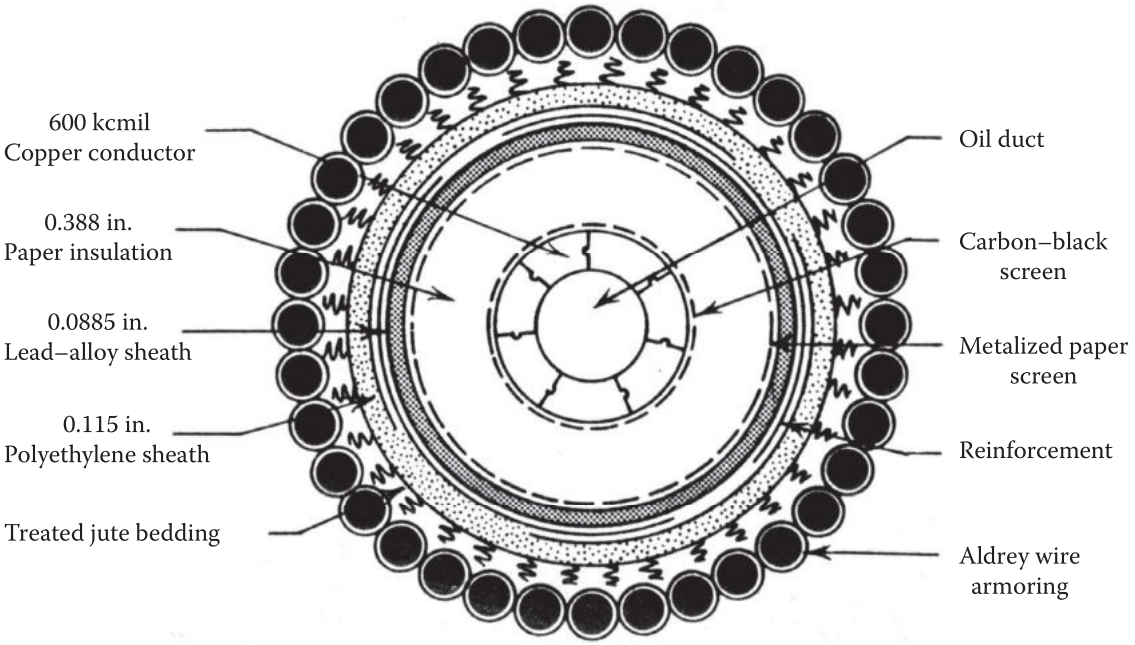

FIGURE 11.7 *Conci* conductors in pressurized oil-impregnated paper submarine cables. (From Gazzana Priaroggia, P. et al. The long island sound submarine cable interconnection, *IEEE Trans.*, PAS-90(4): 1863, 1971.)

effective to counter skin effect in large conductors, and *Conci* conductors are quite effective to adjust the diameter of the oil channel to needs. Thus, a 1600 mm^2 *Conci* conductor reduces the skin effect from 10% to 6% for an increase of the channel diameter from 12 to 40 mm.

Regrouping the strands in segments is another means to counter the skin and proximity effect. The *Milliken* design (Figure 11.4) subdivides the conductor into segments, built up from small strands. The segments are disposed around a steel spiral to form the central channel, kept in place by bronze tapes. Each segment is formed of round wires highly compacted to increase the proportion of metal per unit area of the conductor's cross section. This technique provides a high degree of flexibility to the conductor and is particularly adapted to manufacturing conductors of very large cross section, up to 1300 mm^2, even for pipe-type and polymer cables where the central channel for oil circulation is not required. Increasing the diameter of the central channel of Milliken conductors has little impact on the losses by skin effect since the transposition of the insulated segments (Milliken patent) ensures a uniform distribution of the current within the conductor's cross section.

For gas-insulated cables, the conductor is generally an aluminum tube of appropriate cross section, the dimensions of which are defined by the electric field allowed at the surface of the conductor, while its thickness is optimized with respect to skin effect. An optimal ratio between the radii of the conductor and envelope is generally used. In the case of the semiflexible cable, the conductor is of stranded aluminum wires, while the outer envelope is of corrugated aluminum.

11.2.2.1 Energy Losses

Power transmission by high-voltage cables produces energy losses, which must be kept at an acceptable level. These losses come from different parts of the cable, namely, the conductor, the insulation, as well as the sheath (or pipe). The high power transmission capacity of modern cables requires conductors of very large sections, 3000 mm^2 being the actual limit. They must be economical and meet specific needs of different cable types: flexible, accommodating a channel for the circulation of oil, etc.

Conductor losses: The main source of energy losses comes from the flow of the load current in the conductor, according to

$$W = R_{ac}\, I^2 \tag{11.12}$$

R_{ac} is the ac resistance of the cable conductor, which can be expressed as

$$R_{ac} = R_{dc}\left[1 + K\left(Y_{pe} + Y_{pr}\right)\right] \tag{11.13}$$

where

R_{dc} is the dc resistance of the conductor
Y_{pe} is a factor related to the skin effect
Y_{pr} is a factor related to the effect of proximity
K is a factor characteristic of the type of cable: $K = 1$ for SCOF and 1.7 for HPOF cable

The high value of K in HPOF cable is due to the large magnetic field prevailing in the containing pipe. The dc resistance of the conductor, R_{dc}, is given by

$$R_{dc} = \frac{r_0}{S}\left[1 + a_{20}\left(q_{cmax} - 20\right)\right]\left(1 + Z\right)(W\,m^{-1}) \tag{11.14}$$

where

ρ_0 is the resistivity of the metal at 20°C in Ω–m
S is the cross section of the conductor in mm^2
α_{20} is the coefficient of increment per °C at 20°C
θ_{cmax} is the maximum temperature of the conductor in C
Z is a factor related to the type of conductor ($Z = 0.04$ for large conductors)

Material: From Equation 11.14, it is evident that minimizing the resistive losses requires the use of metals of low resistivity. Among these, copper and aluminum are currently used. The abundance and the relatively light weight of aluminum make it more economical and provide a predominant place in the cable industry. Sodium is another candidate for conductor in high-voltage cables. Its abundance offers interesting possibilities to future high-voltage cables. Its malleability at ambient temperatures allows the sodium conductor to better adapt to deformations subjected to the solid insulation and explains, in part, the good performance of the first sodium cable in the Lima project (Graneau, 1976). However, the highly reactive nature of sodium limits the application of sodium conductor cable to specific cases.

Skin effect: It can be demonstrated that the resistance of a conductor is minimum when the current is uniformly distributed over the entire cross section of the conductor, obtained with dc current. Any operating condition, which modifies the uniformity of the current distribution, necessarily increases the resistance of the conductor and proportionally the resistive energy losses. Due to skin effect, the circulation of an ac current in a conductor forces the current towards the conductor surface. The current density follows an exponential law, having the maximum density at the surface of the conductor, according to

$$J(x) = J_0 \exp\left(-\frac{x}{\delta}\right) \tag{11.15}$$

where
- J_0 is the current density at the surface of the conductor
- δ is the penetration depth
- x is the distance below the conductor surface

The penetration depth δ is a characteristic of the metal and function of frequency f of the ac current, expressed as

$$\delta = \frac{1}{\sqrt{\pi \sigma \mu f}}$$

where
- σ is the conductivity of the metal
- μ is its permeability
- f is the frequency of the current

At power frequencies, the penetration depth in the metals currently used is in the range of centimeter.

The influence of skin effect is particularly significant on large conductors of a radius comparable to the penetration depth at power frequency, reaching 20% increase in the ac losses in a conductor of 1600 mm^2. As mentioned earlier, two approaches are currently used to minimize skin effect: hollow conductor in *Conci* design and segmentation of the conductor in *Milliken* design.

Effect of proximity: Current distribution in the conductors of ac cables, single or tripolar, is affected by the resulting magnetic field produced by current flow in the adjacent conductors, which modifies current distribution in the conductor's cross section, increasing its effective resistance, expressed by a proximity coefficient k_p. Significant proximity effect occurs in pipe-type cables where the high voltage cables are adjacent to one another. To counter proximity effect on the current distribution, the cable conductor is fragmented into segments, which are twisted in range to alternate the position of the cable segments with respect to the adjacent segments, thus redistributing the circulation of the current in the conductor's cross section.

Dielectric losses: Result from the movement of ions across the dielectric insulation and the deformation of the dielectric molecules due to polarization. Good insulating dielectrics leave few ions for the leakage current so that the dielectric loss W_d is mainly related to the polarization of the dielectric molecules, expressed as

$$W_d = UI \cos \varphi \tag{11.16}$$

where φ is the phase angle between the applied voltage U and the leakage current I.

With the following expression of the current, $I = \omega C U$, the dielectric losses can be expressed as

$$W_d = \omega C U^2 \cos\varphi$$

Noting that the angles φ and δ are complementary, for small dielectric losses, one has

$$\cos\varphi = \sin\delta \approx \tan\delta$$

$$W_d = \omega C U^2 \sin\delta \approx \omega C U^2 \tan\delta \tag{11.17}$$

The loss factor tanδ can be expressed as

$$\tan\delta = -\frac{1}{\omega C R} \tag{11.18}$$

where R and C are parallel elements of the insulation impedance.

Equation 11.17 indicates that dielectric losses are proportional to the square of the applied voltage, the cable capacitance per meter, and the frequency of the applied voltage. Gas insulation, less subjected to polarization, gives minimum dielectric losses, related mainly to the presence of epoxy spacers. Polymers, PE and its derivatives, have a loss factor in the range of 1–5 × 10^{-4}. Cross-linking of the PE doubles approximately the PE dielectric losses. Oil-impregnated paper insulation gives highest dielectric losses with a loss factor of about 3 × 10^{-3}.

Sheath and pipe losses: High-voltage cables are provided with a metal sheath to control the distribution of the electric field within the insulation and provide a protective screen against the ingress of humidity and other contaminants. For oil-filled cables, the sheath must also maintain the oil or gas pressure, in the range of 345–450 kPa (50–65 psi). Bronze, copper, aluminum, and lead are among the materials currently used in the manufacture of cable sheath. Lead, in particular, can be made in a continuous sheath to withstand high pressure and to serve as a barrier against infiltration of humidity into the cable insulation. The cable sheath can be made of metal tapes as in the pipe-type cables. Finally, for SF_6-insulated cables, the sheath is usually a rigid steel or aluminum tube, of length of a few tens of meters, fitted with flanges and O-rings at both ends to facilitate their mounting.

Although the cable sheath is not designed to carry load current, proximity of conductors, sheath, or other cables, as well as the multiple grounding points, can give rise to significant induced and ground return currents circulating in the sheath. Practical experience tends to show that significant energy losses are associated with the circulation of leakage currents, which affect the power transmission capacity of the cable.

Ground return current: Occurs when the metal sheath is grounded at more than one point and the low resistance of the metal sheath diverts part of the ground return current through the metal sheath. The ground return current can be significant in single-phase cables, especially if they are well spaced from one another. Grounding the cable sheath at one point only would eliminate the ground return current in the sheath. However, this can result in unacceptable voltage differences along the sheath.

Sheath transposition provides a simple and economical means to reduce the ground return current. Referring to Figure 11.8, showing three consecutive spans of a three-phase cable circuit, the cable sheaths are solidly grounded, at every three joints, and transposed at intermediate ones. Thus, the voltage induced to the cable sheath between two grounding points is the vector sum of three voltage drops Δu_j out of phase by 120° from each other. This voltage will be zero if the cable spans between two joints are equal, resulting in equal induced voltage drops Δu_j, and the ground return current in the sheath would be null. The induced voltage at the sheath increases linearly with the distance from the grounding point to a maximum value at the first intermediate joint; it remains constant between the two intermediate joints and reduces gradually to zero at the next grounding point. In practice, because of the unequal lengths of cable spans between two consecutive joints, the voltages drops Δu_j are not equal, although their vector sum remains small and minimizes the losses from the circulation of ground return current in the cable sheaths. Because of obvious difficulties, this method does not apply to submarine cables. Their sheaths are generally grounded only at both ends of the cable.

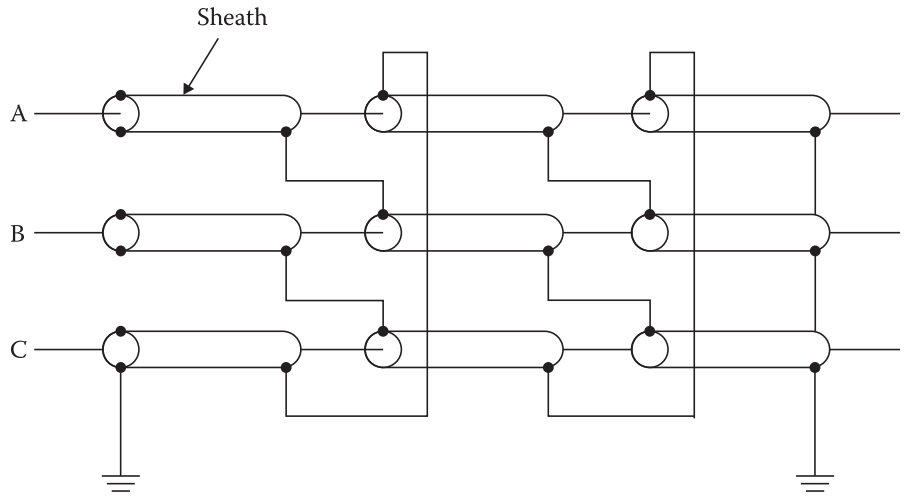

FIGURE 11.8 Cross-bonding transposition of cable sheaths.

TABLE 11.4

Losses (W/m) at Full Capacity of a Three-Phase Circuit Using SCOF Cables

Voltage, kV	Conductor	Sheath	Insulation	Total Losses
33	112.76	14.4	1.2	128.38
66	109.53	14.08	4.41	128.02
132	99.31	15.17	11.62	126.11
275	74.95	21.87	22.61	123.43
400	55.72	22.05	44.58	122.35

Source: Couderc, D. Revue de l'État des Technologies des Câbles de Transport a Très Haute tension en Courant Alternatif et Continu, IREQ report, IREQ, Varennes QC, Canada, November 1987.

Induced currents: Occur when the cable sheath is in proximity of current-carrying conductors and intercepts a part of the generated magnetic flux. The phenomenon is particularly pronounced with magnetic material sheath as in pipe-type HPOF cables. In this case, hysteresis of the metal produces additional losses. These losses by induced currents do not depend on the circuit configuration and can be comparable to the resistive losses in the conductor, thus limiting the transmission capacity of the pipe-type HPOF cables as compared to SCOF cables. Submarine cables are protected by a single- or double-layer armor formed of steel wires to sustain the mechanical stress during the cable laying or removal and protect the cable against mechanical impacts from ship anchors and commercial fishing equipment. Hysteresis losses comparable to those in the cable sheath may develop and reach sufficiently high levels to forbid the use of ferromagnetic materials in the manufacture of the armor.

Table 11.4 gives values of losses originating from different parts in a three-phase cable circuit, composed of three SCOF cables having aluminum conductors of 2000 mm^2 and located at 150 mm center to center from one another. The cables are buried directly in the soil at a depth of 1 m. Corrugated aluminum sheath is transposed and covered with protective PVC sheath (Tareev, 1975). It is noticed that the losses in the insulation increase rapidly with the voltage to reach about 36% of the total losses in a 400 kV cable. Therefore, the temperature rise in the conductor due to dielectric losses becomes a significant factor defining the transmission capacity of a high-voltage cable.

11.2.2.2 Thermal Dissipation

To avoid overheating of the high-voltage cable, it is necessary to ensure adequate dissipation of the losses generated by the cables to the ambient environment. Analysis of the thermal dissipation is made

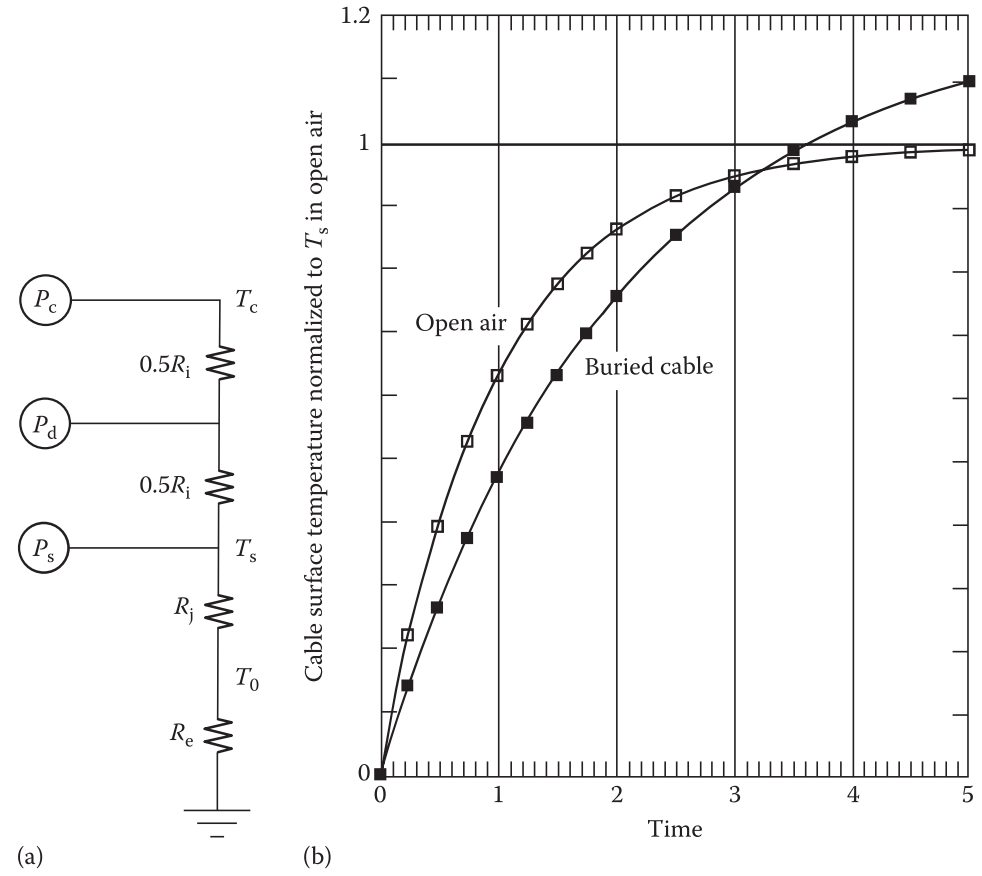

FIGURE 11.9 (a) Thermal equivalent circuit for a cable. (b) Transient responses to a step function energization.

with thermal circuits established from the characteristics of the cable and the soil. Figure 11.9a shows a typical thermal circuit of a buried cable. Thermal sources are identified to the conductor P_c, insulation P_d, and the covering sheath P_s. Thermal resistance of the insulation R_i is divided in two equal parts, separating the three thermal sources. R_j and R_e are thermal resistances of the jacket and soil. Thermal resistances of the metal parts—conductor, sheath, and pipe—are neglected. The solution of the thermal circuit in Figure 11.9a to a step function is of exponential type:

$$\theta(t) = T_f \left(1 - \exp\left(-\frac{t}{\tau}\right)\right)$$

where

θ is the temperature at the conductor
T_f is the terminal temperature
τ is the thermal time constant

Figure 11.9b compares the transient temperature rises of a cable in air with a buried cable following energization of the cable, represented by a step function. It can be seen that the problem is generally more critical to buried cables than those in ambient air: The terminal temperature is higher, and the thermal time constant is longer for the buried cables.

Ampacity: The solution of the thermal circuit determines the ampacity of the high-voltage cable or, inversely, the required dimensions of the conductor corresponding to its transmission capacity. This is out of cope for this book which deals with high voltage phenomena.

Fault conditions: Are rarely determining for dimensioning of cables; it is prudent, however, to verify the cable limits under these conditions. Fault currents expose the cable insulation to the risk of permanent damages, either by electromechanical impacts or by accrued heating of the cable. It is not recommended

to use automatic reclosure in circuits containing high-voltage cables to avoid multiple energization of the fault current. The ampacity of the conductor under fault conditions can be determined by calculating the temperature rise in the conductor according to

$$I_c^2 R_{ac} t_f = A_c \delta C_v \Delta T_c \tag{11.19}$$

where

I_c is the fault current
R_{ac} is the ac resistance of the conductor
t_f is the fault duration
A_c is the cross section of the conductor
δ is the density of the conductor metal
C_v is the specific heat of the conductor metal
ΔT_c is the allowed temperature rise

The thermal dissipation of the soil is neglected due to the short duration of the fault. Furthermore, the limit temperature for thermal instability in the insulation is used as the allowed temperature rise. The resulting cable ampacity under fault condition, in the range of hundreds of kA, is adequate most of the time.

11.2.3 Dimensioning of the Insulation Based on Limit Field (New Cable)

The principal role of the insulation of a high-voltage cable is to maintain the voltage difference between the conductor and sheath over the useful life of the cable. At the same time, it allows the heat generated in the conductor and the dielectric to dissipate in the ambient environment and provides a mechanical support to keep the cable configuration the same over the whole length of the cable. This implies that in addition to the nominal service voltage, cable insulation must withstand transients including lightning and switching overvoltages, which can occur during normal operation. Dimensioning of high-voltage cable insulation is relatively straightforward, namely, by choosing the insulation thickness so that the maximum field intensity within the insulation is maintained below a level selected to meet various stresses related to the operating conditions. It involves three basic steps: selection of the withstand voltage levels, a design field E_0, and determination of the insulation thickness.

11.2.3.1 Selection of the Withstand Voltage Level

It is often the responsibility of the utilities to determine the withstand voltage level in concordance with the operating conditions of the system and various standards available: IEC and ANSI as discussed in Chapter 13. The withstand voltage varies with the nature of the voltage: ac and lightning and switching impulse voltages. However, a specific value for the withstand voltage level can be specified if one knows all the factors contributing to the buildup of overvoltages in the system.

For ac voltage, the designed withstand voltage U_1 is (King and Halfter, 1982)

$$U_1 = k_{sys} \frac{U_n}{\sqrt{3}} = k_1 \, k_2 \, k_3 \, \frac{U_n}{\sqrt{3}} \tag{11.20}$$

where

U_n is the system nominal voltage
k_{sys} is a factor representing the overvoltage that can occur to the cable. k_{sys} can be decomposed into several components k_1, k_2 and k_s explained below.

Typical values of k_i are as follows: $k_1 = 1.15$, a coefficient for the maximum ac overvoltage; k_2, between 1.25 and 1.5, is a factor for the possible variations in the dielectric strength of the insulating material; and for pressurized paper–oil-insulated cables, k_3, between 1.1 and 1.2, is a factor for the variations of the breakdown voltage with the pressure of the impregnating fluid.

TABLE 11.5

Design Impulse Withstand Voltage U_2 for the Calculation of the Insulation of an AC Cable

Nominal Voltage	U_2, kV		
U_n, kV_{rms}	Minimum[a]	Normal	Reduced
110	421	550	450
132	497	650	550
150	560	750	650
220	802	1050	900
380	1356	1550	1425

[a] Minimum values calculated from Equation 11.21.

The withstand voltage for lightning impulse (BIL) as specified by the standard IEC 60141.1 should not be lower than (IEC 60141-1)

$$V_p = 6U_0 + 40 \ (\text{kV}) \tag{11.21}$$

where

V_p is the peak value of the minimum impulse voltage

U_0 is the voltage between the conductor and cable sheath, usually corresponding to the nominal phase-to-ground voltage U_p

However, when the cable is connected to an overhead line, the withstand value V_p according to Equation 11.21 may not be sufficient, and a higher withstand level specified by the standard IEC 60071.1 should be used for the insulation coordination (IEC 60071.1). The designed impulse voltage U_2 used for high-voltage cable is

$$U_2 = k_p \ V_p \tag{11.22}$$

where the coefficient k_p takes account of the nonhomogeneity of the insulation and of the effect of repeated application of impulse voltages on the dielectric strength. The coefficient k_p has generally a value between 1.1 and 1.35 (King and Halfter, 1982).

Table 11.5 gives the values of U_2 for several values of the nominal system voltages U_n. The minimum value is recommended by the IEC for cables with no direct connection to an overhead line, while the reduced values apply to cables directly connected to an overhead line in a system with grounded neutral.

11.2.3.2 Determination of the Design Field, E_0

The insulation thickness can be determined to ensure an adequate distribution of the electric field within the insulation. For a coaxial cable, the field within the insulation is a function of the radial distance according to Equation 11.1 and its maximum value, at the conductor surface by Equation 11.2. Because of the variation of the breakdown field in polymer with the thickness of the insulation and time, the design of cable aims at ensuring a maximum in-service field that the cable insulation can withstand over its whole service life. Let E_1 be the *limit withstand field* measured on new cable samples, discussed in Chapter 7, then the design field E_0 can be defined as

$$E_0 = m_{des} E_1 \tag{11.23}$$

where m_{des} is an empirical coefficient representing the manufacturer's experience in dealing with various factors that affect the limit withstand field of the insulation. m_{des} can be decomposed into several components m_j, less than 1.0. Typical values for m_{des} vary between 0.5 and 0.7.

The limit withstand field E_1 is a propriety of the insulation system used. It depends on the choice of the materials used, quality control, and manufacturing processes and often is manufacturer's proprietary.

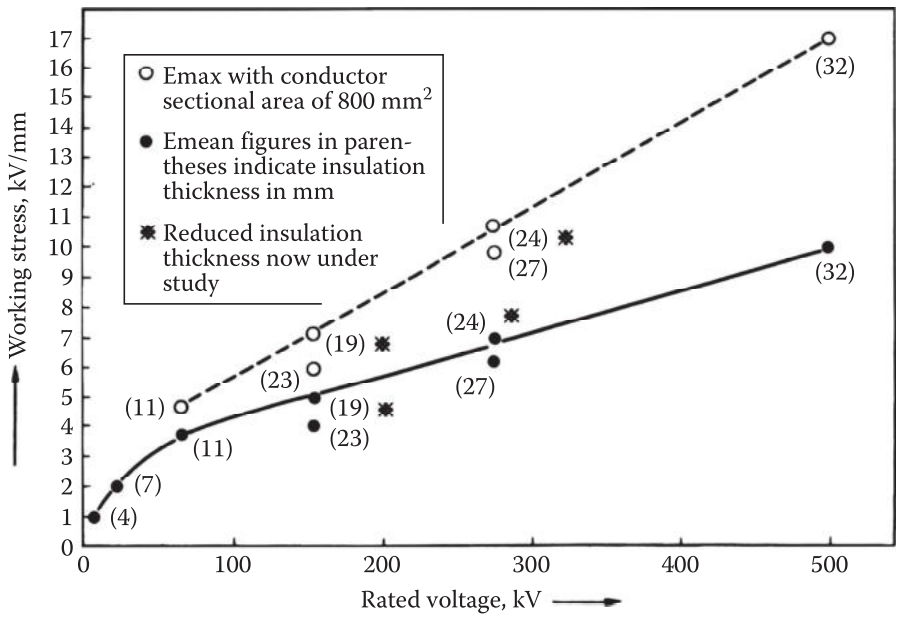

FIGURE 11.10 Variation of working stress as a function of the cable rated voltage. (From Fukuda, T., *IEEE Electr. Insul. Mag.*, 4(6), 15, 1988.)

TABLE 11.6

Typical Design Electric Fields (kV/mm) in High-Voltage Cables

Cable Type	AC, rms	DC Voltage	Lightning	Switching
Paper–Oil	20	35	95	95
PPLP	22		98	
Mass impreg.	—	25	95	90
PE	15		70	
SF_6-insulated	12		25	18
Epoxy	5			

It is possible to have a good idea of the design field E_0 from existing cables, whose dimensions and withstand voltage levels are known. An example is illustrated in Figure 11.10 (Fukuda, 1988a) where the working stress of XLPE cables is given as a function of the rated voltage and insulation thickness (in bracket).

Table 11.6 gives typical limit fields in high-voltage cables for the different types of voltages: ac, dc, and lightning and switching impulse voltages. It can be seen that these typical design fields are significantly below their initial breakdown levels of the insulation to take account of the reduction of the insulation dielectric performances in time.

11.2.3.3 Determination of the Insulation Thickness

Knowing the required withstand levels, the design field E_0 of the cable and conductor dimensions, and noting that for coaxial cables, the maximum field occurs usually at the conductor, given by Equation 11.2, the radius of the envelope can be derived by setting

$$E_{\max} = \frac{U}{\ln\left(b/a\right)}\frac{1}{a} = E_0$$

It follows

$$\ln\frac{b}{a} = \frac{U}{aE_0},$$

which yields

$$b = a\exp\left(\frac{U}{aE_0}\right) \quad \text{and} \tag{11.24}$$

The insulation thickness, e_p, is

$$e_p = b - a = a\left[\exp\left(\frac{U}{aE_0}\right) - 1\right] \tag{11.25}$$

Since both technical specifications and insulation performance vary with the type of voltage stress, Equation 11.25 yields different values for the required insulation thickness. Obviously, the largest insulation thickness should be selected.

Table 11.7 gives typical dimensions of 800 kV cables with different types of insulation and their related characteristic parameters to meet the technical specifications shown in Table 11.8. It can be seen that the design field E_0 evaluated from the cable dimensions and their specified withstand voltages are considerably below the estimated limit field of Table 11.6, to take account of the reduction of insulation dielectric performance due to aging with time in service. These aspects will be discussed in more detail for the three types of cable insulation, namely: Paper-oil in SCOF cables, Polymer in Polyethylene and Cross-link Polyethylene cables and gas in SF_6-insulated cables.

TABLE 11.7

General Characteristics of an 800 kV AC Cable

Cable Design[a]	Unit	SF_6	XLPE	PPL	Paper-Oil
Diameter of central conductor	mm	203.2	60	60	60
Diameter of cable sheath	mm	609	148	121.2	129.3
AC Insulation thickness	mm	203.2	44	30.6	34.65
AC limit withstand field	kV/mm	12	15	22	20
LI limit withstand field	kV/mm	25	70	98	95
SI limit withstand field	kV/mm	18			95
Gas pressure	atm abs	4.5			
Dielectric constant		1	2.2	2.78	3.6
Capacitance per unit length	pF/m	50	135	231	310
tanδ				10×10^{-4}	2.3×10^{-3}
Dielectric losses	W/m			14.53	30
Resistive losses—nominal current	W/m	80		45.2	84.5
Power transmission capacity[b]	MVA	3500	2100	1500	800

[a] Estimated from submissions of manufacturers.
[b] Single phase with natural cooling.

TABLE 11.8

Cable Specifications

General Characteristics	Units	Spec.	SF_6	XLPE	PPL	Paper-Oil
Nominal voltage	kV	765				
Nominal current	A	3000	3000	1500	1500	1500
			Withstand Field (kV/mm)			
AC withstand voltage and withstand field	kV_{rms}	960	4.7	15.8	15.8	15.8
Phase to ground voltage and withstand field	kV	440	2.3	7.6	7.6	7.6
LI withstand voltage and withstand field	kV	1800	8.8	29.5	29.6	29.6
32.58 BIL + 10% and withstand field	kV	1980	9.7	32.5	32.6	32.6
SI withstand voltage and withstand field	kV	1550	7.6	24.5	25.5	25.5

11.3 Aging and Incipient Fault

Operating conditions of high-voltage cables subject their insulation to a variety of stresses, thermal, mechanical, and electrical, which cause irreversible changes in the materials termed as aging discussed in Chapter 7. Insulation failure is caused by incipient faults developing from local failure, causing permanent damage to the insulation system. The net effect is a gradual loss of dielectric withstand, which is generally expressed by the time to failure of the insulation T_b, which is a function of applied stresses, thermal θ, electrical E, etc.:

$$T_b = f(\theta, E) \tag{11.26}$$

The direct consequence to cable design is that cable dimensioning based on the initial dielectric performance of new cable must be validated with respect to insulation aging to ensure an acceptable life expectation T_b. Aging process and hence Equation 11.26 vary, however, with the insulation. This will be further discussed in the following regarding the main aging processes: thermal, electrical and environmental with reference to the three general insulation systems currently used in high-voltage cables.

11.3.1 Self-Contained Oil-Filled Cables

11.3.1.1 Thermal Aging

Early studies of thermal aging by Montsinger (1930), followed by Dakin (1948) discussed in Chapter 12, have shown that thermal aging follows the Arrhenius' chemical rate theory, according to

$$T_b = A\exp\left(\frac{B}{\theta}\right) \tag{11.27}$$

where

T_b is life expectation
θ is the temperature in K
A and B are constants determined by the activation energy of the particular chemical reaction responsible for thermal aging

Equation 11.27 shows up as a straight line when the logarithm of the insulation life is plotted against the reciprocal of the absolute temperature, known as the Arrhenius' life curve.

Decomposition by-products: Thermal aging breaks chemical bonds, gradually reducing the structure of the cellulose molecules to H_2O, CO_2, CO, and furans or furfuraldehydes (Burton et al., 1984; Shroff and Stanett, 1985). Furans are uniquely related to the degradation of paper and, hence, can be effectively used to monitor its aging process in paper. The decomposition of the insulating oil produces a variety of by-products, namely, carbon, H_2, CH_4, C_2H_2, C_2H_4, and C_2H_8. They are currently used in their diagnostics. The degradation rate depends on the presence of moisture, oxygen, ions, metal, reaction products, and additives.

11.3.1.2 Electrical Aging

Electrical aging is caused by development of PDs, which erode the insulating material, forming a permanent path along the discharge channel in the paper insulation. Even that filling with the impregnating fluid, provides improved dielectric strength, discharge channel constitutes a weak point of the insulation, by which subsequent discharges can develop in a treeing process. The discharge channel extends gradually in time to eventually bridge the gap and cause the final breakdown of the insulation, at voltages much lower than the initial value obtained in new samples.

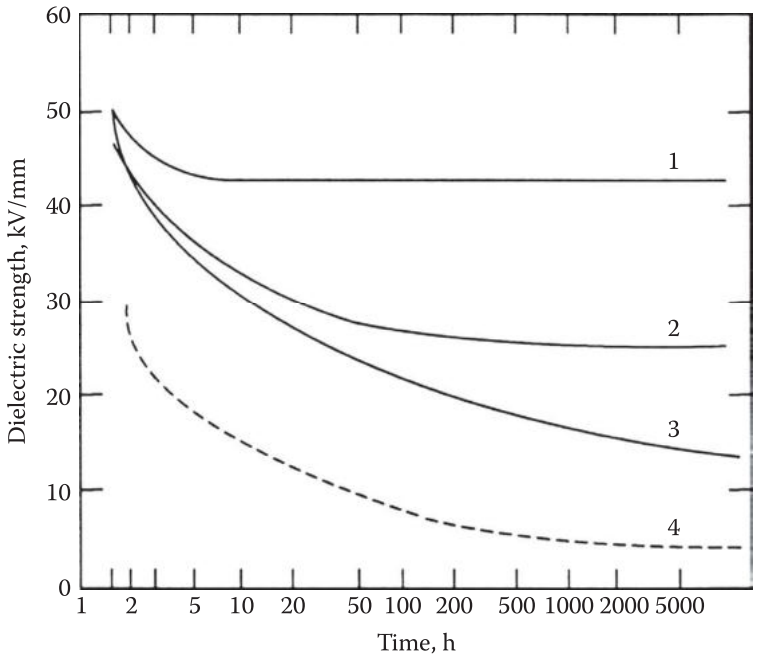

FIGURE 11.11 Life curves of different types of ac-impregnated paper–oil cables. (1) SCOF cable (130 kPa), (2) pressurized gas cable (1500 kPa), (3) mass-impregnated cable, and (4) nonpressurized three-phase cable (nonradial field). (From Couderc, D. Revue de l'État des Technologies des Câbles de Transport a Très Haute tension en Courant Alternatif et Continu, IREQ report, IREQ, Varennes QC, Canada, November 1987.)

Figure 11.11 shows life curves of different types of paper–oil insulation. It can be seen that there is a decrease in the breakdown field with time, from the initial short-term breakdown field E_d to a final long-term value E_∞, which may be expressed by the following empirical relation (Couderc, 1987), a variant of the inverse power law, applied to the paper–oil insulation of oil-filled cables subjected to a constant ac voltage:

$$E_d = E_\infty + \frac{\Delta E}{\sqrt[n]{t_b}}, \text{ which can be rewritten as} \tag{11.28}$$

$$\frac{E_d - E_\infty}{\Delta E} = \frac{1}{\sqrt[n]{t_b}} \tag{11.29}$$

where
E_d is the disruptive field
E_∞ is the withstand field
ΔE and n are experimental constants depending on the properties of the insulation
t_b is the time to breakdown

Equation 11.29 expresses the reduction of the residual dielectric strength $E_d - E_\infty$ with time, which is more convenient to determine the end of life of the insulation system: the service life of the equipment is completed when the residual dielectric strength of its insulation is lower than an acceptable level above the operating stresses to minimize in-service failure.

Figure 11.12 shows variations of the final values of the breakdown field E_∞ of paper insulations pressurized in oil and gas, as a function of pressure for different values of paper thickness. It illustrates the effectiveness of oil impregnation in improving the dielectric strength of the impregnated paper–oil insulation, as discovered early by Emmanuelli.

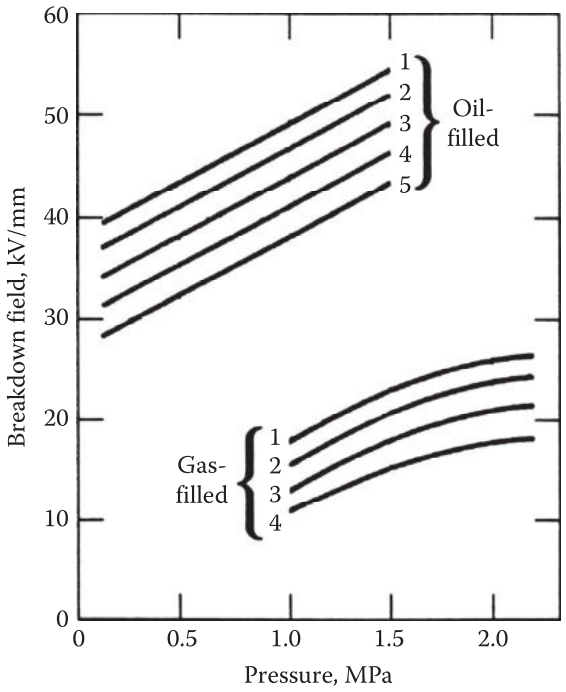

FIGURE 11.12 Long-term ac dielectric strength of paper–oil as a function of the pressure, for different paper thickness: (1) 0.03, (2) 0.045, (3) 0.075, (4) 0.125, and (5) 0.175 mm. (From Couderc, D. Revue de l'État des Technologies des Câbles de Transport a Très Haute tension en Courant Alternatif et Continu, IREQ report, IREQ, Varennes QC, Canada, November 1987.)

11.3.1.3 Environmental Aging

Oil-filled cable forms a closed system, usually by means of a lead or aluminum sheath, which can withstand the high oil pressure of several thousands of kPa. The metallic sheath also constitutes a protective barrier against environmental aging and, in particular, ingress of moisture. However, it also favors accumulation of the PD decomposition by-products within the insulation. Saturation of the dissolved gas in oil must be avoided to prevent the development of PDs within the cable insulation and further enhance the aging process.

11.3.2 Polymeric (PE and XLPE) Cables

11.3.2.1 Thermal Aging

The low loss factor tanδ of polymeric insulation, such as PE and XLPE, tends to minimize the effect of thermal aging. However, the compact design of cables may favor local thermal aging in areas with poor cooling for the cables. Furthermore, the morphological structure of the material also influences the aging process. PE, which is thermoplastic, may soften under heat. This, in turn, tends to favor the displacement of the cable conductors subjected to a local mechanical stress, and failure may occur as a result of the loss of adequate insulating clearance. XLPE, which is thermoset, will harden under heat and becomes brittle as a result of aging.

11.3.2.2 Electrical Aging

The electrical aging mechanisms—PDs, electrical treeing (ET), water treeing (WT), and charge injection—occur at contaminants, defects, protrusions, and voids (CDPV) and tend to be localized. The development of electrical trees starts from one of CDPV sites, erodes the dielectric forming voids in the insulation, grows within the bulk of the insulation until it bridges the gap separating the electrodes, and causes breakdown (Denseley, 2001). In the process, it generates PDs, the signature of which may be detected at terminal points for diagnostic purpose.

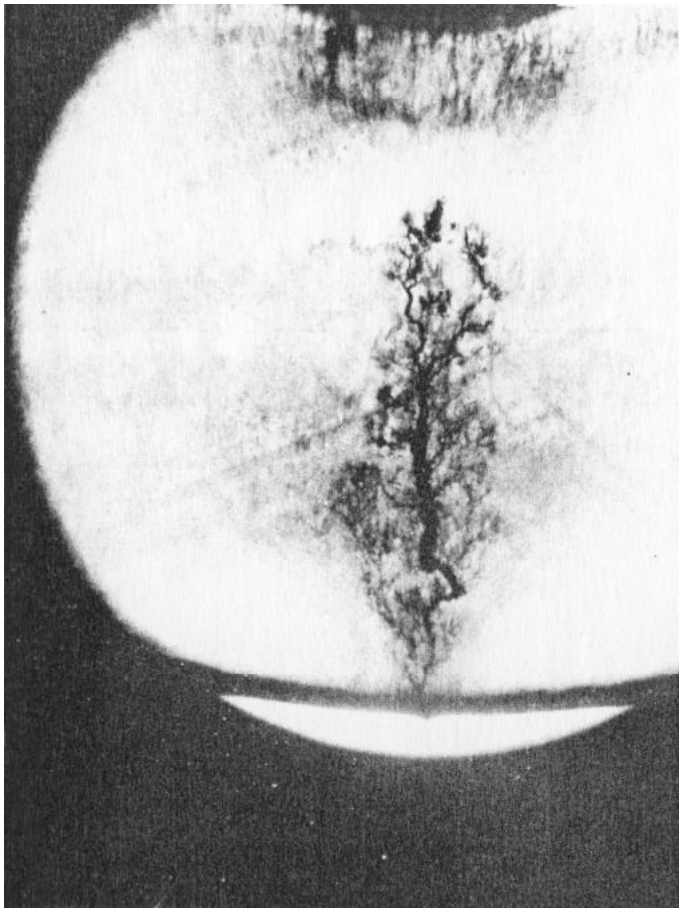

FIGURE 11.13 Electrical trees. (From Lawson, J.H. and Thue, W.A., Summary of service failure of high voltage extruded dielectric insulated cables in the United States, in *IEEE International Symposium on Electrical Insulation*, Boston, MA, June 1980, pp. 100–104.)

Electrical tree: Two mechanisms tend to explain the development of trees in polymer dielectrics (Figure 11.13):

1. One assumes that breakdown of the chemical bonds in the molecules liberates enough energy to form a gas-filled channel in the dielectric, which eventually joins the two electrodes. Breakdown of the gas channel follows and leads to failure of the solid dielectric.
2. The other theory assumes that treeing results from PDs developing within the gas-filled voids in the dielectric. The action of PDs contributes to erosion of the dielectric and formation of channels.

Contradictory observations tend, however, to minimize the importance of PDs in the treeing process, in favor of the combined action of electric charges captured within the dielectric and the breakdown of molecular bonds.

Three phases of tree development related to initiation, propagation, and final breakdown of the insulation can be distinguished:

Initiation of tree: An electrical tree can develop from a protrusion at the surface of the conductor or cable shield, or a contaminant, or void within the insulation, which causes local enhancement of the electric field sufficiently high to initiate PDs. Eventually, the insulation may be locally destroyed, forming an empty channel along the discharge paths.

Propagation of tree: The mechanism of propagation of an electrical tree may be explained by the formation of gas-filled cavities by the PDs. Such a channel constitutes a cavity of low dielectric

constant, which accentuates the local electric field and perpetuates the development of PDs within the cavity. Decomposition of the insulation gives rise to carbon deposits on the wall of the discharge channels, which tends to extend the conductor potential into the insulation or to accentuate the field enhancement ahead of the tree branching, thus favoring the progression of the tree further into the insulation.

Final breakdown: Occurs when the electrical tree completely bridges the insulation to form a conducting path and hence a short circuit between the central conductor and the cable sheath. The fault current that follows is sufficiently high to permanently damage the insulation. It is probable that the development of incipient faults is accompanied with PDs sufficiently high to be detected outside the cable insulation and constitutes a subject of discussion still open. The difficulty to detect incipient faults resides in the intermittent nature of PDs. In effect, the development of PDs also deposits charges on the walls of the cavities forming tree branches. It reduces the local electric field within the cavities and suppresses PDs. The process can resume again when the deposited charges are sufficiently neutralized.

Life estimation: The aging of polymer-insulated cables, corresponding to a gradual reduction of the dielectric withstand of the cable insulation, follows an inverse power law

$$E(t) = E_0 \frac{1}{t^n} \tag{11.30}$$

where

$E(t)$ is the withstand field for a stress duration t

E_0 is the withstand value for a unit duration

Taking the logarithm of both sides of the preceding equation yields

$$\ln\left[E(t)\right] - \ln\left(E_0\right) = -n \ln t \tag{11.31}$$

which expresses a linear relationship between the logarithm of the ratio $E(t)/E_0$ and the time t that the insulation is subjected to the ac stress.

Figure 11.14 shows the variations of the withstand field of a 66 kV XLPE cable, as a function of time under a constant ac voltage (Fukuda, 1988a). It can be seen that the withstand field is reduced by a factor of 1.4 over a period of 30 years, passing from an initial value of 40 kV/mm to 25 kV/mm. The corresponding value of the exponent n is 15 for the XLPE-insulated cable insulation. Similar results were obtained with impulse voltage.

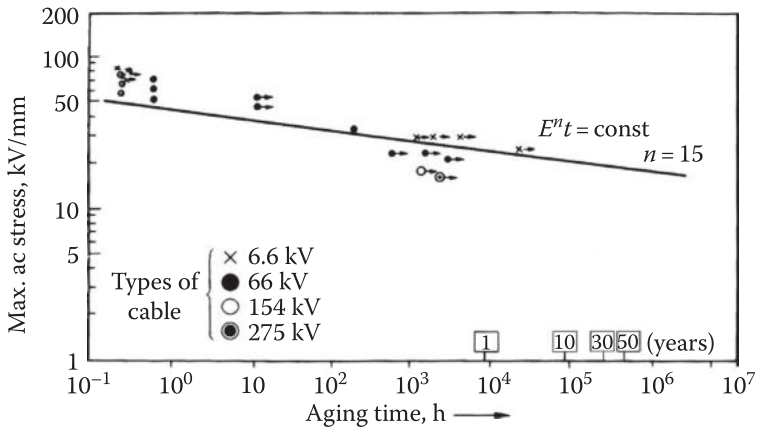

FIGURE 11.14 Aging test of XLPE-insulated cables. (From Fukuda, T., *Electr. Insul. Mag.*, 4(5), 9, 1988a.)

Possible mechanisms for electrical aging in polymer: In spite of the general consensus about development of incipient faults via water and electrical trees, there is still no adequate physical mechanism explaining the inverse power relationship observed in electrical aging data. Several mechanisms have been advanced for the initiation of the aging processes in polymeric insulation.

Bahder et al. (1982) proposed a model based on the scission of molecular chains and the formation of craters at discharging voids to explain the aging of polymer. The development of PDs in microvoids of dimensions less than 100 μm, already present within the bulk polymer, produces ion space charges that penetrate the polymeric insulation in the immediate surroundings of the microvoid. It is the back and forth movement of the ion space charges dictated by the applied ac field that causes the breaking of molecular chains to form microcracks, branching outwardly from a stem. The same process contributes to enlarge the stem and cause the microcrack branching to extend farther into the polymer and transform it into an electric tree. The time to breakdown of polymer-insulated cables may be expressed as

$$t_b = \frac{1}{f b_1 \left\{ \exp\left(b_2 \left(E - E_{th}\right)\right) - 1 \right\} \exp\left(b_3 E_b\right) + b_4} \tag{11.32}$$

where

f is the frequency of the ac test voltage

b_1, b_2, b_3, and b_4 are constants representing the dependence of polymeric material on temperature, shape, and frequency of the applied voltage (ac, dc, or impulse)

E and E_b are the applied and breakdown field, respectively

The threshold stress E_{th} is influenced by the type and shape of the imperfection and by the temperature of the insulation.

Figure 11.15 illustrates the variations of the logarithm of voltage stress as a function of logarithm of time to breakdown. It can be seen that the breakdown field follows the inverse power law at high stresses. However, at low stresses close to the operating values, the breakdown occurs at shorter times than predicted by the inverse power law.

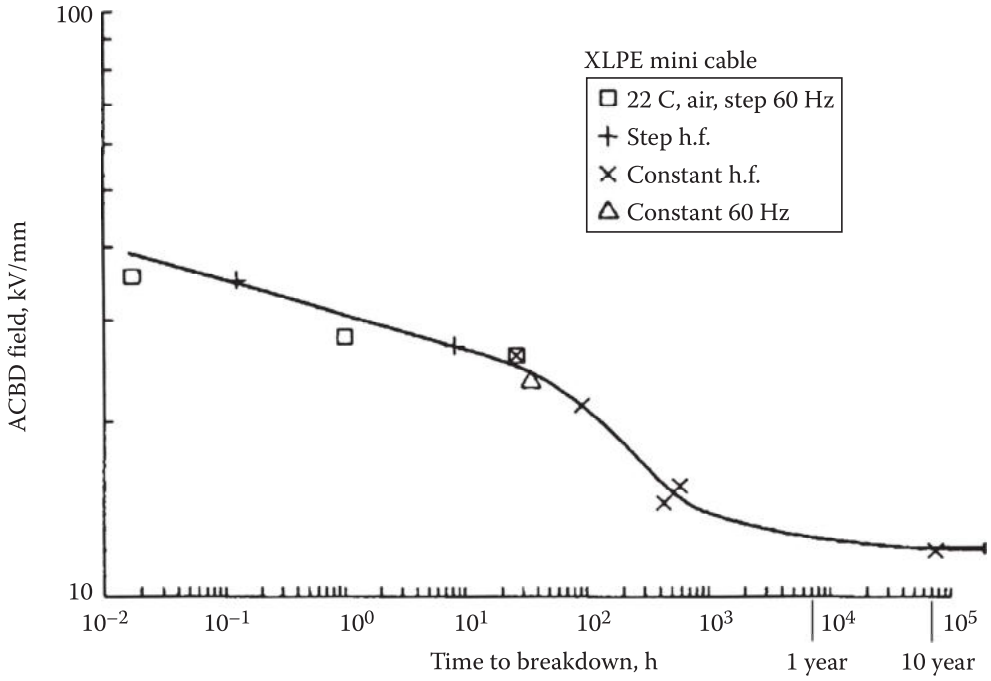

FIGURE 11.15 Variation of the ac breakdown field with time to breakdown—results from Bahder et al. (1982). (From Dang, C. et al., *IEEE Trans. Dielectr. Electr. Insul.*, DEI-3(2), 237, 1996.)

Crine (Crine, 1987; Dang et al., 1996; Parpal et al., 1997) proposed the rate theory to explain the aging process in polymers, especially regarding its behavior at field intensities close to the normal operating value of the cable. Crine assumed the following:

- The final breakdown occurs when charge carriers go over an energy barrier of height ΔG and width λ. The nature of the energy barrier is typical of the insulation tested.
- The electric field reduces the height of the energy barrier and affects the barrier width λ.
- Breakdown is a thermally activated process.
- A general relationship was derived for the time to breakdown t_b as related to the field E, the energy barrier ΔG, and λ:

$$t_b = \frac{2h}{kT}\exp\left(\frac{\Delta G}{kT}\right)\csc h\left(\frac{e\lambda E}{2kT}\right) \tag{11.33}$$

At high field intensities, the preceding expression simplifies to

$$t_b = \frac{4h}{kT}\exp\left(\frac{\Delta G}{kT} - \frac{e\lambda E}{2kT}\right) \tag{11.34}$$

where
k is the Boltzmann constant
h the Planck constant
e the electron charge

which predicts an exponential relation between field and time to breakdown.

Thus, ΔG and λ can be readily deduced from the intercept and the slope of the curve E as a function of the logarithm of time. Figure 11.16 presents the results of Figure 11.15 using semilogarithmic paper however, showing variation of the breakdown field as a function of logarithm of time. It can be seen that the breakdown field follows an exponential law at high fields before it tapers off at low stresses.

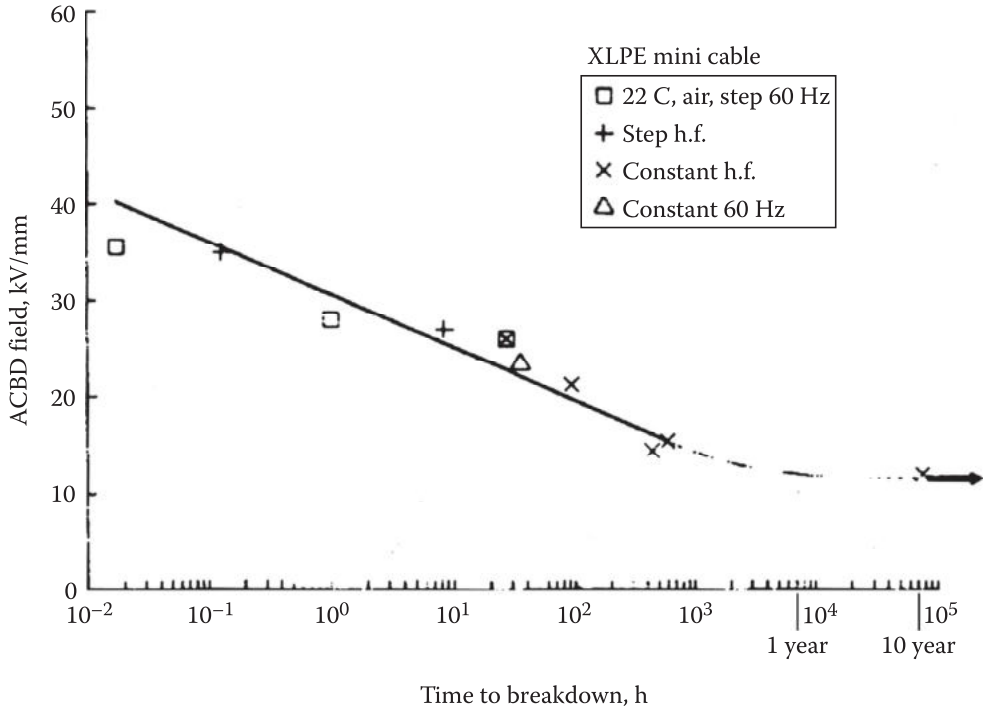

FIGURE 11.16 Variations of the ac breakdown field with time to breakdown—results from Bahder et al. (1982). (From Dang, C. et al., *IEEE Trans. Dielectr. Electr. Insul.*, DEI-3(2), 237, 1996.)

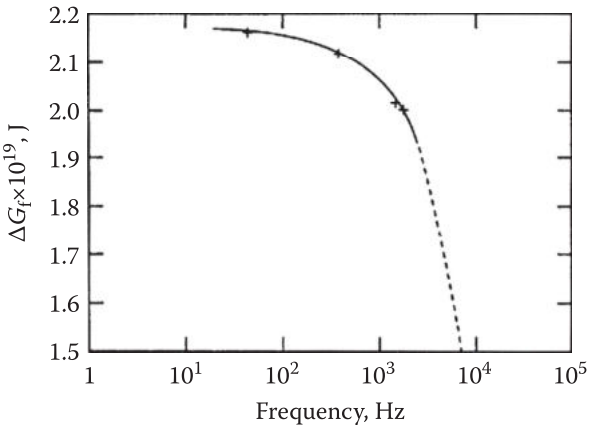

FIGURE 11.17 Variations of ΔG as a function of the frequency of the applied field at 22°C by Bahder et al. (From Parpal, J.L. et al., *IEEE Trans. Electr. Insul.*, EI-4(2), 197, 1997.)

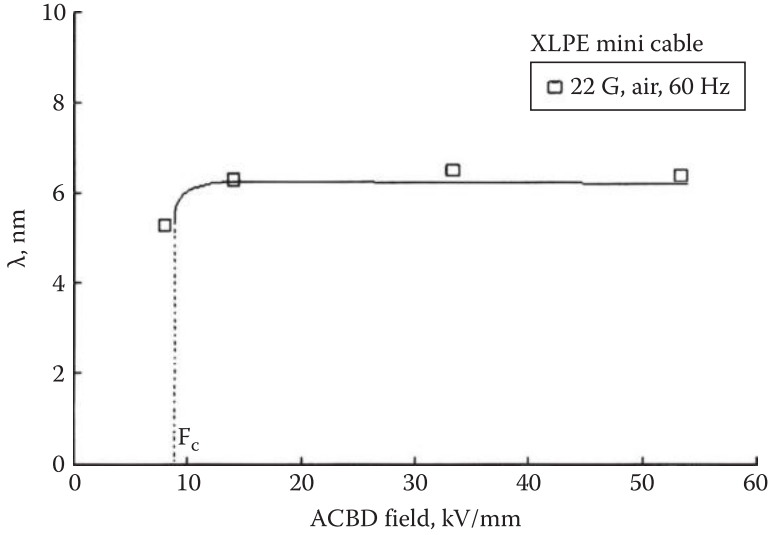

FIGURE 11.18 Variations of λ as a function of the applied field. (From Parpal, J.L. et al., *IEEE Trans. Electr. Insul.*, EI-4(2), 197, 1997.)

Evaluation of Δ*G* and λ (Figures 11.17 and 11.18) shows that at high field intensities, λ is constant while it sharply decreases at low field values. This variation of λ at low fields explains the taper off observed in the curve of electrical aging as a function of aging time.

11.3.2.3 Environmental Aging

Polymeric insulation is particularly sensitive to humidity, which favors development of water trees within the insulation. Steamed cure seems to produce water-filled voids within the insulation, thus favoring development of water trees. Migration of humidity through the protecting jacket into the main polymeric insulation of power cables is another cause, which is particularly present in distribution cables, due to the flooding of the cable manhole, which can immerse the cable insulation over long periods. The best way to counter the ingress of humidity is to use a hermetic metallic, lead or aluminum, sheath. The solution comes with a price and is limited to high-voltage cables of 200 kV and higher. Finally, on-site installation of cable joints and terminations is still the weak points in a cable system regarding ingress of moisture.

Water trees: When cables are in a humid environment, as often is the case with underground cables, the development of electrical trees is often preceded by the development of water trees (or chemical trees when chemical substances are present in the water). The development of water trees seems related to the migration of water molecules through the protective jacket into the main PE insulation. Like electrical trees, water trees are attracted by the electric field: they develop from protrusions at the conductor and metal sheath or from

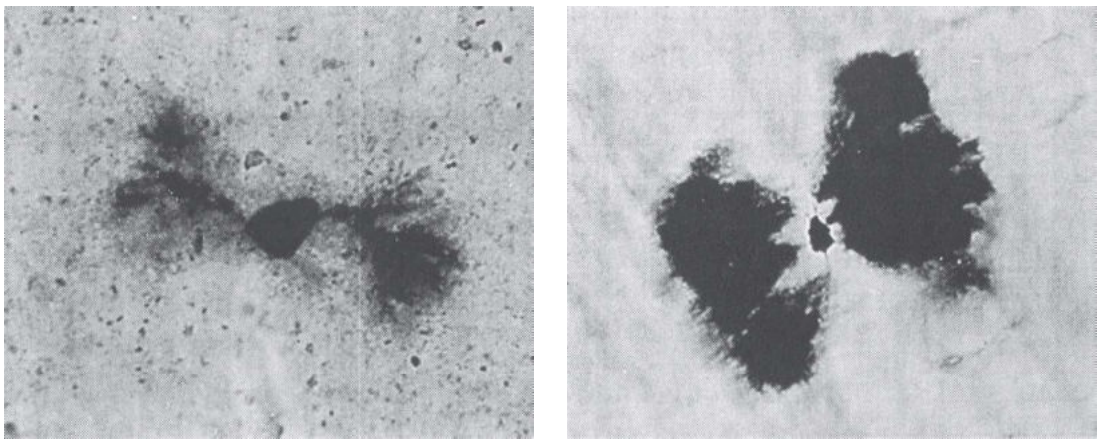

FIGURE 11.19 Water trees developing from a solid contaminant. (a) A typical bowtie tree in XLPE cable insulation aged eight months at three times rated voltage. (b) A bowtie tree in clay filled EPR cable insulation, initiating from a contaminant. (From Boggs, S. and Xu, J., *Electr. Insul. Mag.*, 17(1), 23, 2001.)

solid impurities within the dielectric, giving rise to butterfly tie trees. Water trees are diffuse, however, with no clear evidence of forming well-defined channels (Figure 11.19). The structure of the water trees takes the form of a series of water-filled voids, which are interrelated by oxidized tracks (Moreau et al., 1993).

Water trees seem to be not as permanent as electrical trees. In effect, drying the insulation can temporarily remove water trees and allow the insulation to recover most of its dielectric strength. However, water trees will quickly reemerge when the dried cable is put back into a humid environment, indicating that water trees do weaken the insulation, making their paths easy for the migration of water molecules within the insulation. Water trees do not directly cause failure of cable insulation, which occurs after a transition of water trees into electrical trees. Four development phases of water trees can therefore be distinguished, related to the initiation, propagation, transition to an electrical tree, and final breakdown of the insulation (Figure 11.20).

Initiation of water tree: Starts from a location in the insulation where the local field enhancement is sufficiently high to attract water molecules, probably due to their dipole polarization, to initiate water trees. The natural locations for field enhancement are protrusions at the conductor and cable sheath, empty or gas- or liquid-filled cavities formed during the curing process, especially steam cured, or subsequent to a separation of insulation at the interface with the conductor or cable shield.

Propagation: It may be expected that the high permittivity of water also creates local concentration of the electric field in the dielectric around the water-filled void, which is comparable to field enhancement around a conducting contaminant of the same shape and size. Field enhancement around water-filled void attracts new water molecules and allows the water tree to grow. However, the high dielectric constant of water also reduces proportionally the electric field within the water-filled void, making the development of PDs within the water-filled voids practically impossible. As a result, water trees can progress further into the insulation but do not directly cause breakdown.

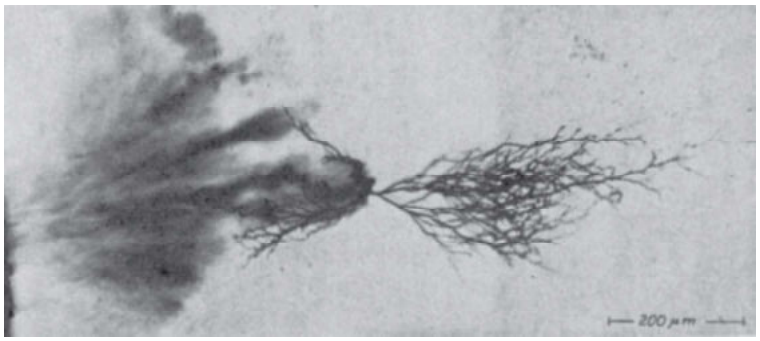

FIGURE 11.20 Transition of water tree to electrical tree from a vented water tree. (From Kalkner, W. et al. Water treeing in PE and XLPE insulated high voltage cables, *International Conference on Large High Voltage Systems*, CIGRE, paper no. 21-07, 1982.)

Transition to electrical tree: It may be assumed that once a water tree succeeds to bridge the two electrodes, a conduction current may flow in the water-filled channel, causing vaporization of the water and thus transforming it into a gas-filled channel. Water vapor having a lower dielectric strength, combined with the high electric field across the tree channel, can initiate PDs, transforming it into an electrical tree.

Final breakdown: Once the transition from water to electrical tree has occurred, the final breakdown phase is identical to that of an electrical tree when it completely crosses the insulation to form a conducting path and hence a short circuit between the central conductor and the cable sheath. The fault current that follows is sufficiently high to permanently damage the insulation.

11.3.2.4 Decomposition By-Products

Although PDs and chemical reactions do produce decomposition by-products in polymeric insulation, they cannot be collected or measured and hence cannot be used in assessment of the polymeric insulation.

11.3.3 Gas (SF_6)-Insulated Cables (Lines)

Due to their great ability to regenerate from their decomposition by-products, and since the majority of the decomposition by-products associated with PDs are in gaseous state and have comparable dielectric performances as the gas itself, gases do not practically age. Aging of gas–solid insulation is therefore determined by the aging of insulating spacers and other supporting structures, forming an integrant part of the insulation.

11.3.3.1 Thermal and Mechanical Aging

Gas insulation is little affected by thermal aging due to the low value of the loss factor tanδ and the usually large physical dimensions of gas-insulated equipment, which provides adequate heat transfer to ambient air. However, the cyclic expansions and contractions of the conductor with loading conditions do wear off the metal, producing particles, which may be detrimental to the insulation.

11.3.3.2 Electrical Aging

Since breakdown of gas–solid insulation generally occurs along the gas–solid interface, incipient fault in solid insulation, normally associated with the development of electrical trees within the bulk of the solid insulation, although a possible cause for failure of insulating spacers, is rather unlikely to occur due to the low electric field in the bulk of epoxy spacer. A more likely cause of failure is associated with the development of surface tracking, related to the development of steady PDs at the spacer–gas interface. Erosion of the epoxy resin leaves a path partially covered by carbon deposits, which constitutes an easy path to PDs to propagate along the interface and, eventually, cause the breakdown of the spacer. Surface tracking is dependent on the formulation of epoxy resin and of the type of filler used. Resistance to surface tracking is generally used as a criterion for evaluating insulating material used in the manufacture of spacers.

Life estimation: Several investigations have been made to evaluate the long-term behavior of epoxy insulators in full size as well as reduced-scale samples (Crucius and Luxa, 1980; Honda, 1984). Figure 11.21 shows the voltage–time characteristics of reduced-scale epoxy postinsulators, subjected to accelerated aging with the applied voltage being the accelerating parameter (Nitta and Kuwahara, 1981). The results evaluated over a period of several hundred hours show a reduction rate of the dielectric withstand of the insulators of about 3% per decade of time. The aging seems to follow an exponential law corresponding to the linear relationship between the breakdown field and the logarithm of time to breakdown.

Possible aging mechanism: Several mechanisms have been advanced for the aging mechanism in polymeric insulation, principally for PE and XLPE. For SF_6–epoxy insulation, Dakin and Studniarz (Dakin and Studniarz, 1978; Studniarz and Dakin, 1982) observe that aging of cast epoxy resin may be associated with the development of PDs in the bulk epoxy volume. This mechanism explains the existence of

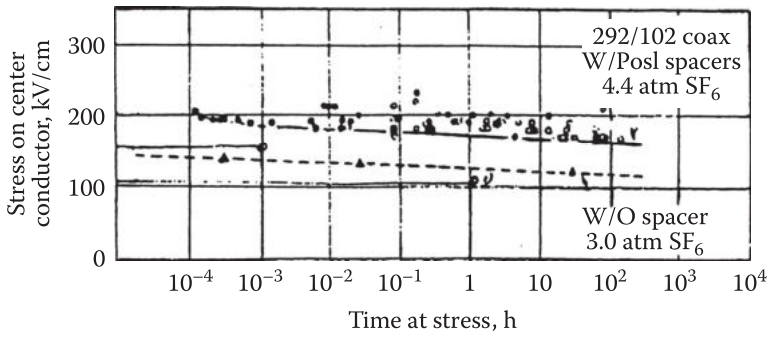

FIGURE 11.21 *V–t* characteristics of molded epoxy spacers. (From Nitta, T. and Kuwahara H., *IEEE Trans. Power Appar. Syst.*, 100(6), 3055, 1981.)

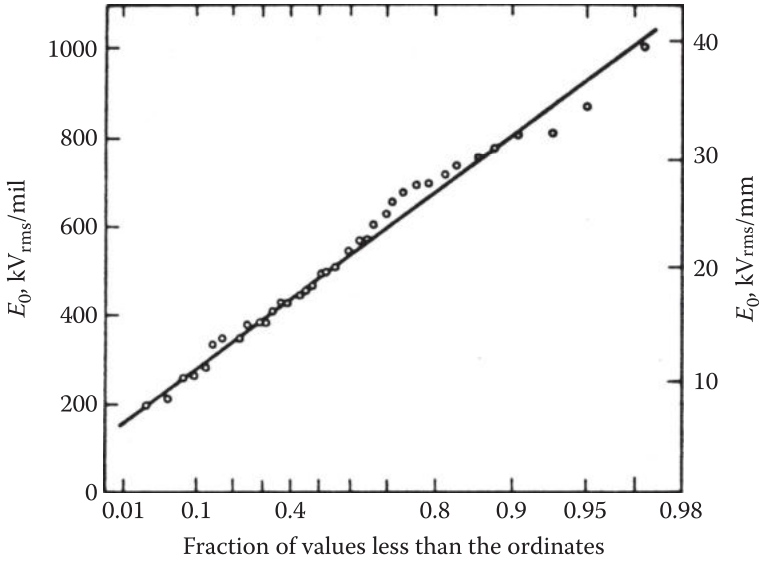

FIGURE 11.22 Extreme value distribution of the onset fields for PDs E_0 in epoxy spacers. (From Dakin, T.W. and Studniarz, S.A., The voltage endurance of cast epoxy resins. *IEEE International Symposium of Electrical Insulation*, 1978.)

a threshold field E_0 below which no PD can be initiated and hence no aging is experienced by the epoxy at fields below E_0.

Figure 11.22 shows variations of the onset field E_0 for PDs plotted in extreme value statistics graph paper. The threshold field for epoxy is estimated to be about $E_0 = 6$ kV/mm. The time to failure can be expressed as a function of the electrical stress E, or more precisely the differential field $(E - E_0)$, according to

$$t = \left(\frac{1}{E - E_0}\right) K_2 \exp\left[-K_1 (E - E_0)\right] \tag{11.35}$$

taking the logarithm of both sides gives

$\ln t = \log\left(\frac{1}{E - E_0}\right) + \ln(K_2) - K_1 (E - E_0)$, which can be rewritten as

$$\ln t = K_2 - K_1 (E - E_0) + \ln (E - E_0) \tag{11.36}$$

where K_1 and K_2 are experimental constants.

Figure 11.23 illustrates variations of electric field as a function of time to breakdown, using a semilog graph paper. A linear relationship between the two parameters for high values of the electric field can be observed. However, the curve tapers off at low field intensities approaching the normal operating stress.

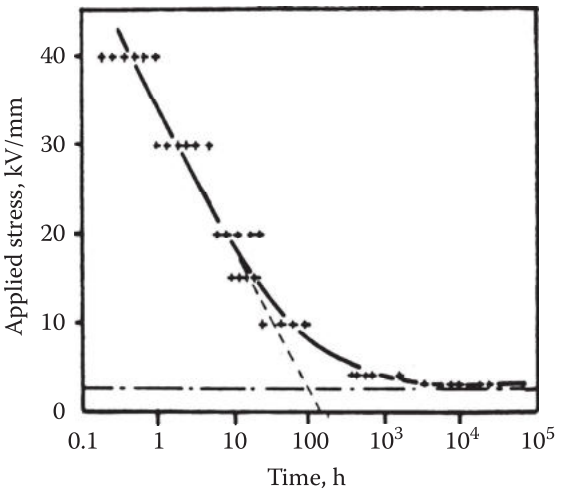

FIGURE 11.23 Electrical aging—semilog. (From Cygan, P. and Laghari, J.R., *IEEE Trans. Electr. Insul.*, EI-25(5), 923, 1990.)

11.3.3.3 Environmental Aging

Compressed gas insulation is subjected to ingress of humidity through the joints and particle contamination associated with the cyclic expansion–contraction of the conductor, producing metallic particles and mechanical vibrations, which may set loose particles from their natural traps.

Decomposition by-products: There are no significant gaseous by-products associated with the degradation of SF_6 and epoxy insulators. As a result, there has been little interest to develop methods for assessing the aging state of gas insulation via their decomposition by-products. Analysis of the gas is, however, made prior to major work requiring the opening of the gas-insulated equipment, especially current interrupting devices such as circuit breakers and disconnecting switches.

11.3.4 Experimental Evaluation of Life Function

The lack of satisfactory theories for various aging processes combined with the fact that practical insulation systems are simultaneously subjected to multiple aging processes has promoted alternative approaches to estimate the life, or remaining life, of the insulation from experimental tests. However, the problem turns out to be one of the most difficult and has not been fully mastered in spite of the considerable research work already undertaken in this field.

11.3.4.1 Accelerated Aging Tests

Accelerated aging tests are frequently used to evaluate the long-term performance of an insulation system. Introduced some 60 years ago by Mathes (1948), the concept of evaluating insulating materials in their operating environment with one or two accelerating parameters is well accepted and widely used nowadays. The objective is to obtain experimentally the life curve of the insulation system subjected to high stresses and to extrapolate the results to the operating conditions. It assumes basically that the failure mechanism under the specific test conditions will remain the same over the range of variations of the accelerating parameters.

Electrical and thermal stresses are the most commonly used as accelerating aging parameters. Time to breakdown was measured as a function of the accelerated parameters, starting at high stresses while keeping the other parameters constant. The source frequency is another accelerating parameter. The logic behind this approach is the assumption that PDs are sensitive to being alternately initiated and suppressed within a half cycle of the applied voltage. Increasing the frequency of the test voltage would then accelerate the aging process in a proportional manner. Aging tests are regularly conducted with ac voltage frequency ranging up to several kHz.

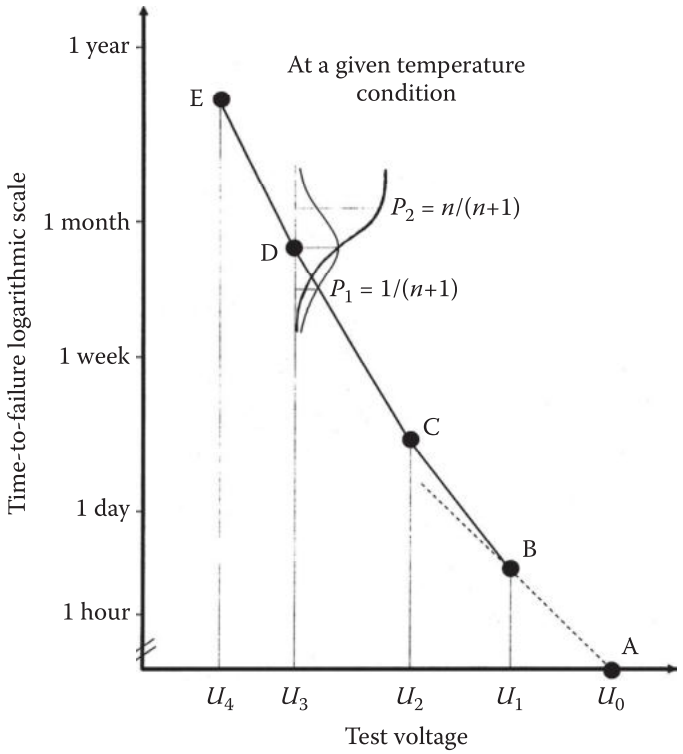

FIGURE 11.24 Typical schedule for a conventional endurance test program. (Dang, C. et al., Dielectric performance of distribution XLPE-cable accessories at high temperatures, CEA report 139-D-505A, 1990.)

Typical endurance test method: Referring to the schematic test schedule of Figure 11.24, the life curve is obtained in *M* test series; each consists of subjecting *N* test samples to constant stresses and measure the time (or number of voltage applications for impulse voltage) to failure of all the samples. The accelerating parameter (applied voltage) is then changed to the next level, and the test repeated with a new group of *N* samples. For practical reasons, the aging test usually starts with the highest voltage level, which produces failures of test samples in relatively short time. The test voltage is then reduced in subsequent test series to gradually approach the operating stress. At each test voltage level, the measured population of *N* values of the time to breakdown can be evaluated for its defining parameters, for example, mean value and standard deviation. The experimental life curve is defined by the set of *M* mean times to breakdown. It is then extrapolated for the service life of the insulation system.

11.3.4.2 Analysis of Data

With the previously mentioned test procedure, the time to failure at any test voltage is defined by a statistical distribution for a population of *N* samples. Two situations are possible, corresponding to uncensored and censored data.

Uncensored data: Correspond to the situation when all the samples in a test series fail, usually corresponding to test under relatively high stresses. The data are termed uncensored, and the probability distribution of the time to breakdown is defined between the two extreme probabilities (Chapter 3):

$$P_{\min} = \frac{1}{N+1} \quad \text{and} \quad P_{\max} = \frac{N}{N+1}$$

Different statistical functions can be evaluated regarding their adequacy to represent the experimental data. *Normal* and *Weibull* distributions are most frequently used. Their parameters are determined from the experimental distribution of the time to failure.

Censored data: As the voltage level is reduced, the test duration and the possibility that a test series will contain samples that do not breakdown both increase. The data are then termed censored (Nelson, 1978), and the probability distribution of the time to failure is defined between the two extreme probabilities:

$$P_{\min} = \frac{1}{N+1} \quad \text{and} \quad P_{\max} = \frac{N_b}{N+1}$$

where $N_b < N$ is the number of failed samples in the test series.

The distribution of the time to failure of censored data is necessarily less accurate as N_b is smaller than N. For practical reasons, N_b should be at least equal to the number of parameters defining the specific statistical distribution function: two in general for *normal* and *extreme value* functions and three for *Weibull* distribution.

To avoid censored data, several alternatives have been considered, namely, residual dielectric strength and residual life.

Residual dielectric strength: Provides an alternative to remedy the unpredictable duration of the conventional endurance test. In this approach, the endurance test is carried out in the same manner as with conventional endurance test. However, the residual strength of the insulation is evaluated at the end of an aging test series, determined by the schedule test duration or the time until the first failure occurs, whichever event coming first (Montanari et al., 1984). In this way, variation of the aging state of the insulation defined by its residual dielectric strength with the aging duration can be derived. The advantage of this approach is obviously the possibility to set a time limit to the endurance test. Also, since the residual strength is evaluated for all the test samples of the series, there are no censored data involved, and the analysis of the test data may be simplified.

Residual life: Although both the time to breakdown and the residual strength are complementary parameters for assessing the aging process of an insulation system, there is no simple relationship between the two. Evaluation of both the actual state of the insulation and its residual life of polymer-insulated cable after it experiences a (first) failure in service provides an interesting approach to estimate the remaining service life of a practical cable system (Gotoh et al., 1984). It provides some correlation among the actual in-service aging (up to the first failure), the actual state of the insulation, and the estimated remaining life established by accelerated aging tests (which necessarily take less time than a conventional endurance test on new cable samples).

11.3.4.3 Optimization of Test Parameters

The destructive nature of aging tests, combined with the fact that the test samples may be limited in number, has promoted the need to optimize the aging test procedure. The following considerations should be made:

- Aging test corresponds essentially to extrapolation of test results obtained under high-stress conditions to estimate the service life of the insulation at the normal operating stresses. It assumes that the breakdown at low stresses follows the same mechanism at high stresses.
- The total number of test samples, $N_t = N \times M$, depends on the desired accuracy of the distribution of the time to breakdown, limited between the extreme probabilities $P_{\min}$ and $P_{\max}$, which determine the number of test samples for each test series, and the number M of test voltages, which determines the effective extent of the experimental life curve.
- The testing time increases with reduced test voltage. In conventional endurance tests, where the time to breakdown is measured, a test voltage selected too close to the normal operating stress may easily result in testing time exceeding the scheduled limits, with consequences either on the test budget or as most often is the case the termination of the test with censored data.
- Minimize the number of censored data.
- Real-time update of the experimental life curve may be made and allows proper adjustment of the next test voltage level to maximize the chance of completing the test series within the allowed time.

11.4 Gas-Insulated Substations

Gas-insulated substations (GIS) are the natural outcome of the development of a variety of gas-insulated switchgear in the first half of the twentieth century. Figure 11.25 illustrates the basic scheme for a GIS: a set of disconnecting and measuring equipment, which allow appropriate changes of circuit configuration. All equipment shares the same insulation system, which also includes bushings for connections to power transformers, overhead lines, and/or underground cables. Connections between the various pieces of equipment are made with short bus sections. Gas barriers are used to isolate the breakers and disconnecting switches from the main gas insulation, protecting it from particles produced during switching operations. GISs are usually arranged in breaker bays, disposed in two areas of high and low voltages, located at both sides of power transformers.

While the operation of GIS is no different from a conventional substation, the good dielectric performance of gas insulation allows a reduction in size by a ratio of about 1/10. Combined with the low risk of fire hazards and minimum visual impact, GIS can be installed in urban areas, where the high cost of land has practically forbidden the installation of conventional substations. However, GIS does have some particular problems related to operation of disconnecting switches, namely, fast transients, ground potential rise, and trapped charges. These aspects of GIS will be discussed in the following.

11.4.1 Generation of Fast Transients

One of the features of SF_6 insulation is that breakdown time is much shorter in SF_6 than in air, which generates transient voltages with very fast front (Boggs et al., 1982). The problems are particularly prevalent in GISs during operations of disconnecting switches because of the high number of restrikes, and the reduced dimensions of GIS cause transient reflections occurring at higher rate with little attenuation.

Figure 11.26 compares voltages at the source and load sides of the switch during an opening operation. It can be seen that, as the contacts of the switch are separated, restrikes occur each time the voltage difference between the source and the load exceeds the withstand level of the gap between the contacts, increasing with the gap distance until it withstands the source voltage.

Short-time breakdown characteristics: Referring to Figure 11.27, each restrike between the contacts of the switch corresponds to the injection of a step voltage V_0 equal to the restrike voltage, which separates into two transient waves of half amplitude, propagating away from the injection point (Fujimoto et al., 1982). The transient wave and its subsequent reflections within the GIS can build up substantial overvoltages of short front times, in the range of tens of nanoseconds, that are applied to the GIS insulation. Two principal problems are related to the fast transient voltages: the breakdown characteristics of SF_6 insulation at a short time to breakdown and the transient ground potential rise higher in GIS than in conventional substations.

Because of the rather flat V–t characteristics of SF_6 insulation, the choice of protection devices for gas-insulated equipment is made assuming a V–t curve remaining constant at the BIL level of the equipment down to breakdown times around 1 μs, before an increase in the breakdown voltage at shorter time to breakdown. This explains the tendency to use SF_6-insulated metal-oxide lightning arresters for the overvoltage protection of gas-insulated equipment.

Transient potential ground rise: Because of the very fast front transient impulses, the penetration depth into the metal conductor and envelope is small (Fujimoto et al., 1982). The internal and external surfaces of the envelope behave as two distinct concentric conductors connected together at the open end of a connection to the overhead line, which constitutes a triple junction access point (Figure 11.28). In presence of the inductance of the ground loop, the circulation of such a ground current generates a transient ground potential rise higher than those encountered in conventional substations. Research work sponsored by the Canadian Electrical Association (CEA) on the subject led to the conclusion that with appropriate means to limit the inductance of the ground loop, this situation does not constitute a danger to maintenance personnel (Ford et al., 1982). On the other hand, these potential rises can be critical to substation control and measuring equipment (Dick et al., 1982).

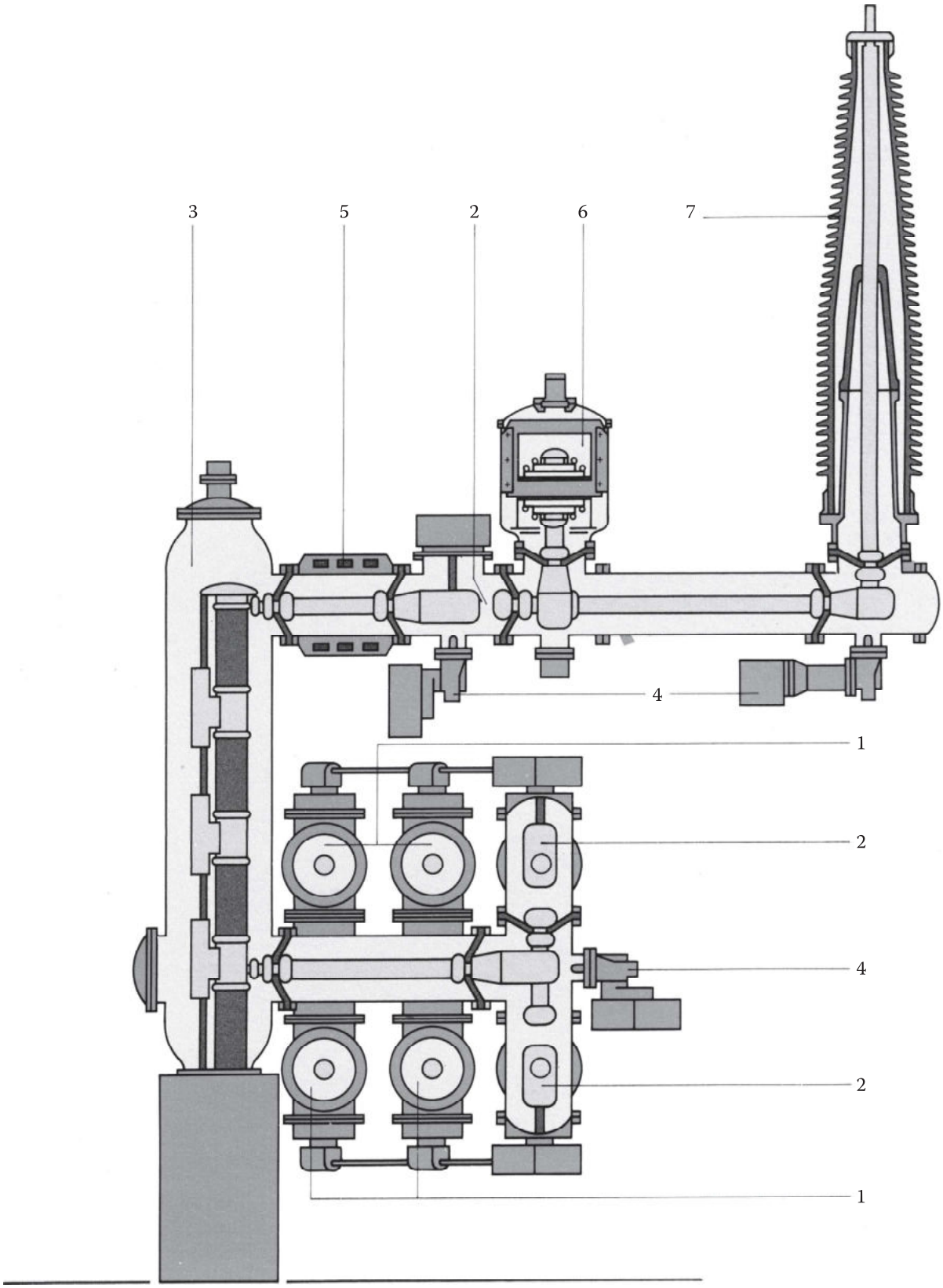

FIGURE 11.25 Basic components of a GIS. (1) Busbar, (2) disconnecting switch, (3) circuit breaker, (4) earthing switch, (5) current transformer, (6) voltage transformer, and (7) outdoor bushing. (From ABB Ltd., SF_6 Gas-insulated switchgear—Type ELK, 1990.)

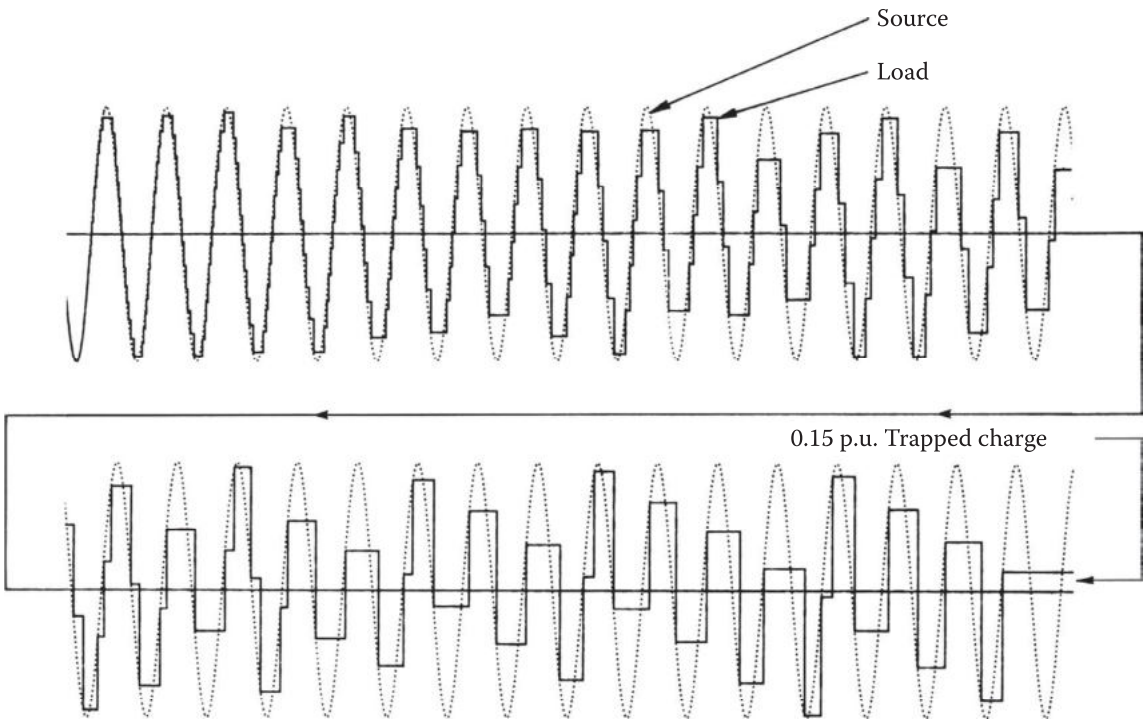

FIGURE 11.26 Restrikes between contacts during opening of a disconnecting switch. (From Boggs, S.A. et al., *IEEE Trans. Power Apparatus Syst*., PAS-101, 3593, 1982.)

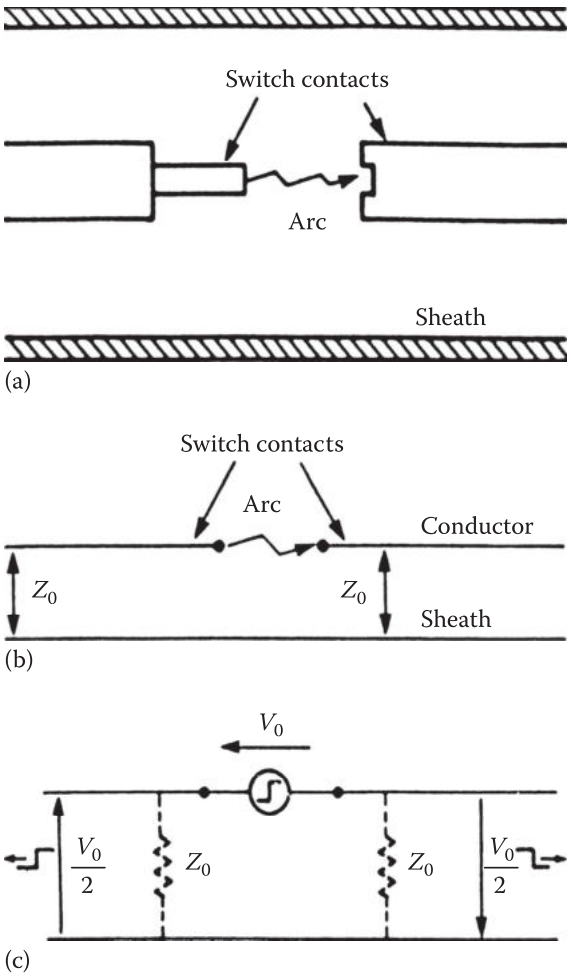

FIGURE 11.27 Generation of fast transients. (a) Arcing between contacts. (b) Circuit representation of arcing between contacts. (c) Propagation of transient voltage. (From Fujimoto, N. et al., *IEEE Trans. Power Apparatus Syst*., 101, 3603, 1982.)

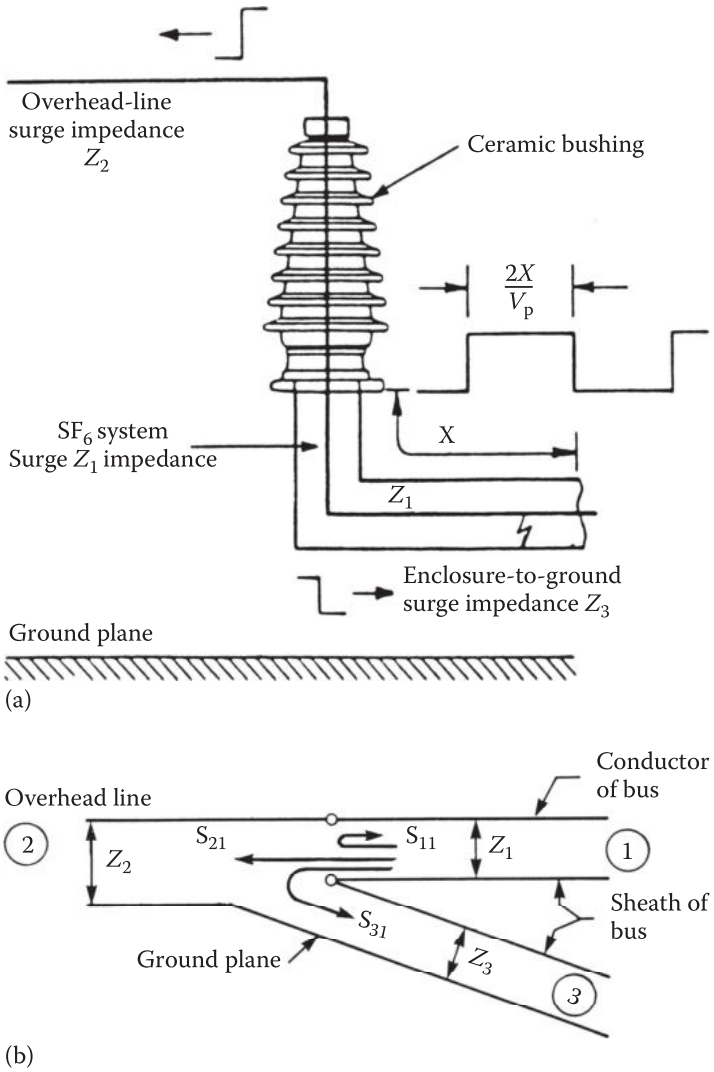

FIGURE 11.28 Mechanism of ground potential rise. (a) Physical arrangement of GIS connection to overhead line. (b) Circuit representation by a three-port transmission line. (From Fujimoto, N. et al., *IEEE Trans. Power Apparatus Syst.*, 101, 3603, 1982.)

Grounding: Solutions have been proposed and some are already incorporated in the grounding design of GISs (Dick et al., 1982):

- Grounding at several points, with shorter spacing between the grounding points near the terminations to overhead lines where the highest overvoltages (of the range of several kV) are possible (Dick et al., 1982).
- Special grounding, using a ground plane, is installed at the base of wall bushings and cable terminations.

Trapped charge: Because of the random nature of arc quenching in SF_6-insulated disconnecting switches, electrostatic charges may be trapped at the conductor and insulating spacers after the opening of the switch, as illustrated by the recording of the voltage across the contacts shown in Figure 11.29 (Boggs et al., 1982). The presence of trapped charge at or near the insulating spacer may affect the local distribution of the electric field and cause its failure.

11.4.2 Risk of Burn Through

Operating SF_6-insulated equipment raises some concerns regarding the possibility of burn through of the envelope, subsequent to a phase-to-ground fault. Service experience to date has shown that the design of

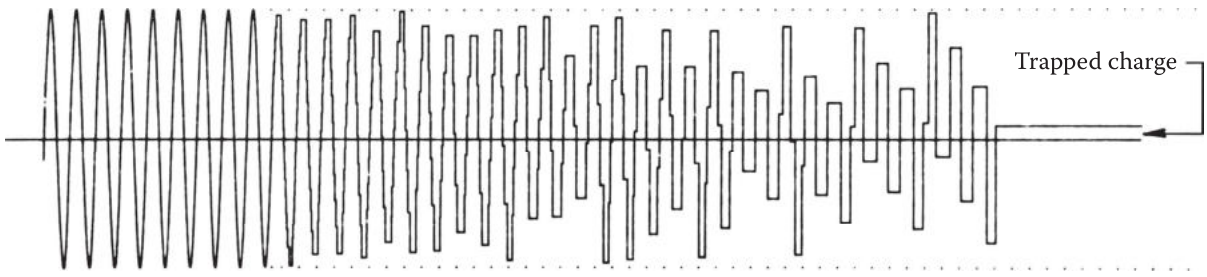

FIGURE 11.29 Trapped charge. (From Boggs, S.A. et al., *IEEE Trans. Power Apparatus Syst.*, 101, 3593, 1982.)

gas-insulated equipment is secure in this respect. Burn through is a rare incident, which, even if potentially dangerous due to the spilling of SF_6 (discussed in Chapter 4), has not caused problems to operating personnel. It occurs only when the arc initiated by the fault has moved close to a spacer and remained stationary for sufficiently long time to melt the metal, causing burn through of the envelope. On the other hand, evaluation of the risk of burn through (Trinh, 1992) of gas-insulated cables has shown that these risks are one to two orders of magnitude lower than those associated with the failure of the cable, typically of the range of 10^{-6}–10^{-8}. Furthermore, the risk of burn through can be controlled during design of the equipment and protection system by the use of rupture discs, which control gas ejection and minimize the risk of injuring personnel.

11.4.3 Special Considerations for Operating Gas-Insulated Equipment

Although SF_6-insulated equipment operates in a contained environment, it is sensitive to ambient changes, especially when the GIS is located in open air. In the following, the main factors that can influence its operation are reviewed.

11.4.3.1 Temperature

In general, temperature has little effect on dielectric performance of gas insulation, which is rather determined by the gas density (as discussed in Chapter 4). However, there exist situations where a change in temperature does cause a change in the gas density and hence can affect the dielectric performances of the gas-insulated equipment.

Low temperatures: Operating gas-insulated equipment at very low temperatures can cause liquefaction of the gas, which, in turn, can considerably reduce the gas density and hence the withstand strength of gas insulation. Figure 11.30 presents the ranges of pressure and temperature for which SF_6 remains in the gaseous state. It can be seen that, for the range of pressures currently used (4–5 bars), the temperature limit for a safe operation of gas-insulated equipment is −40°C.

Mixtures of SF_6 and N_2: The use of SF_6–N_2 mixtures at a slightly higher pressure constitutes an elegant solution to avoid the liquefaction of pure SF_6 while maintaining an adequate dielectric performance of gas insulation. The partial pressure of SF_6 is selected so that the lowest operating temperature remains above its liquefaction threshold, while the added N_2 compensates for the reduced withstand value of SF_6 at reduced partial pressure (Cookson and Pedersen, 1978; Wooton and Chantry, 1980). However, it should be noted that the arc-quenching capability of the mixture is practically reduced proportionally to the partial pressure of SF_6.

Temperature difference: When a gas volume is subjected to a temperature difference, at equilibrium, this imposes a gradient of the gas density within the gas volume (Trinh, 1982) as discussed in Chapter 4. This results in a reduction of the dielectric withstand of the gas insulation, which is a function of the lowest gas density within the compartment. Properly compartmentalizing the gas-insulated bus with a gas-barrier spacer installed at the building wall will resolve this problem.

11.4.3.2 Humidity

In spite of the self-contained environments of GIS, it is observed that water can be absorbed in aluminum and, particularly, in epoxy spacers. Subjected to variations of ambient temperature, humidity continuously

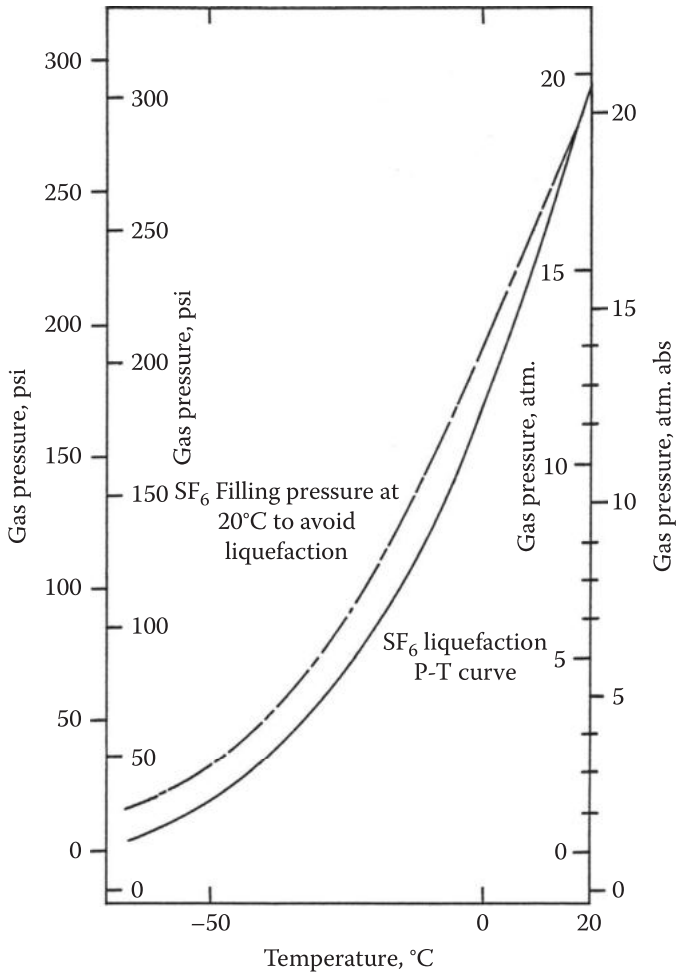

FIGURE 11.30 Characteristics of change in state of SF_6. (Trinh, N.G., Consideration of the effect of a temperature gradient on the dielectric performance of a CGI bus, *IEEE International Symposium on Electrical Insulation*, Philadelphia, 183, 1982.)

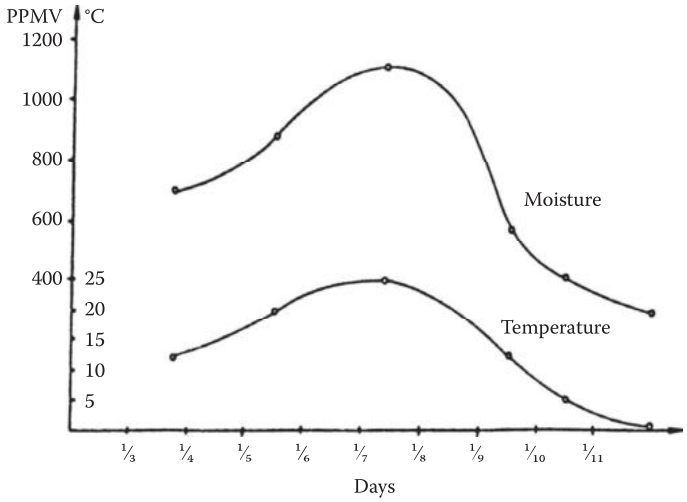

FIGURE 11.31 Seasonal variations of humidity in gas-insulated equipment carried out at the Norwegian Institute of Technology. (From Chu, F.Y. and J-M. Braun. *Assessment of Moisture in Gas-insulated Substations*. Canadian Electrical Association, report No. 217 T 424, October 1989.)

exchanges between the gas, spacers, and aluminum conductor and envelope, giving rise to a seasonal variation of humidity within the gas-insulated equipment as shown in Figure 11.31 (Chu and Braun, 1989).

These variations of humidity, combined with the wide range of temperatures to which gas-insulated equipment may be exposed, have resulted in the establishment of strict limits concerning the acceptable level of

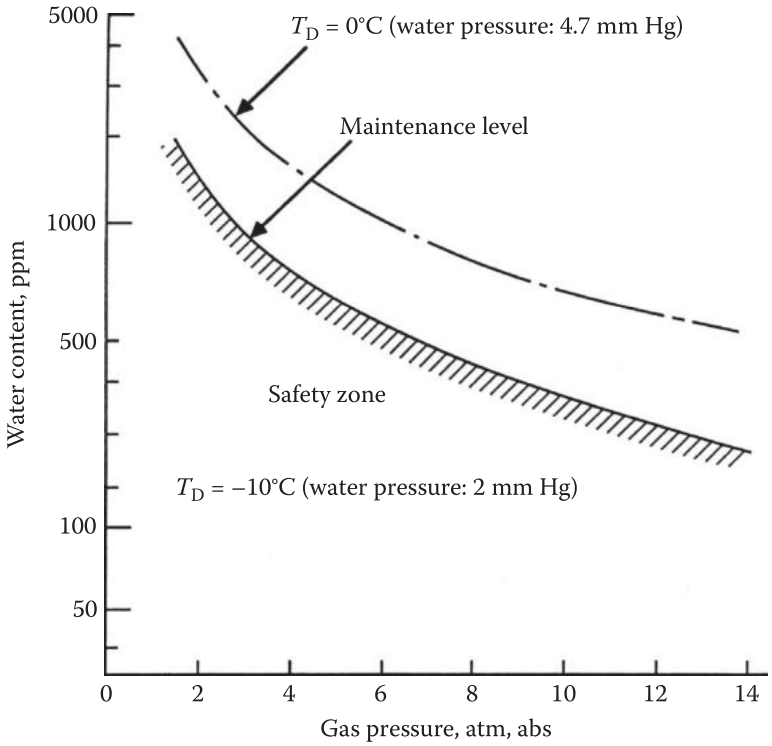

FIGURE 11.32 Recommended limits for the acceptable levels of humidity in gas-insulated equipment. (From Chu, F.Y. and J-M. Braun. *Assessment of Moisture in Gas-insulated Substations*. Canadian Electrical Association, report No. 217 T 424, October 1989.)

humidity. Schmidt recommends maintaining the relative humidity level in the gas-insulated equipment to keep the dew-point temperature below the lowest temperature encountered in service (typical dew-point temperature is −10°C) to avoid formation of liquid water at the gas/spacer interface (Schmidt and Szente, 1974). Figure 11.32 summarizes the recommendations regarding the admissible level of humidity for gas-insulated equipment. These are generally more strict for disconnecting equipment due to the presence of SF_6 decomposition by-products, which are more sensitive to humidity. Typically, a level of 65 ppm at 4 atm abs is recommended for equipment operating at temperatures as low as −40°C (Chu and Braun, 1989).

11.5 Accessories

High-voltage cables comprise relatively short sections, joined together to meet the required length. In addition, to connect the cable to either the overhead line or other equipment, terminations and bushing are also required. The distance between two joints, determined by the length of the cable in a reel, varies with the dimensions and type of cable. It can be in the range of hundreds of meters for impregnated paper–oil and polymer-insulated cables. It is only a few tens of meters for rigid gas-insulated cable imposed by the limits of transportation. Both joints and terminations are specific to the type of cable and must be built up on-site, which requires qualified technical personnel and particular working conditions regarding cleanliness and well sheltering from adverse weather conditions. Design principles for the basic accessories, straight joint and termination, are discussed in the following for the three insulation systems: paper–oil, polymer, and SF_6 insulation.

11.5.1 Impregnated Paper–Oil Accessories

11.5.1.1 Principal Types of Accessories

Impregnated paper–oil-insulated accessories are the most widely used, either as straight joints to extend a cable length, or terminations to connect the cable to overhead line conductor or other pieces of

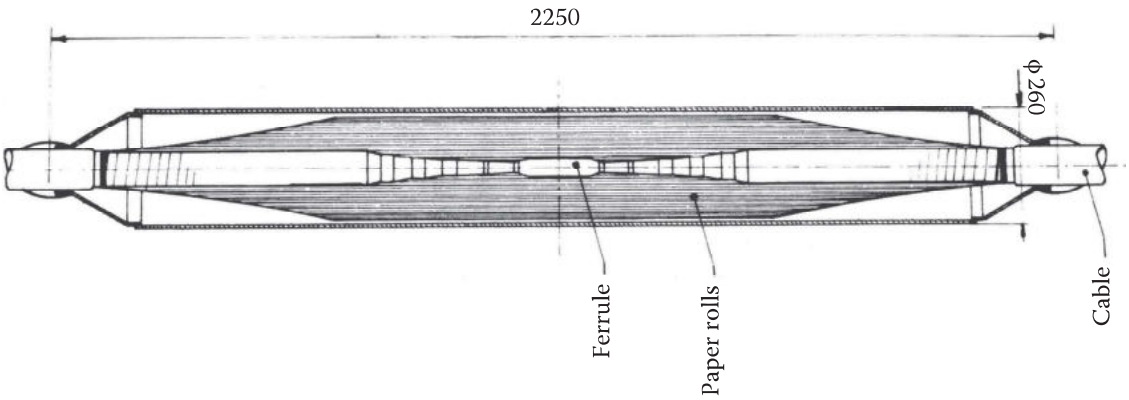

FIGURE 11.33 Illustration of cable straight joint. (From Luoni, G. et al., *IEEE Trans. Power Apparatus Syst.*, PAS-100(1), 174, 1981.)

equipment, or wall bushing. Impregnated paper–oil-insulated accessories are sometimes used in conjunction with gas-insulated equipment or polymer-insulated cables.

Sectionalized straight joints: Are used to extend the length of a cable or to repair a failed cable. The design of a straight joint is necessarily symmetrical, connecting two identical cable sections. To build up a cable straight joint, it is necessary to complete the electrical and hydraulic circuits before building up the insulation of the joint, generally at the detriment to its physical dimensions, which can reach two to three times the diameter of the cable. Figure 11.33 shows a typical arrangement of a cable straight joint. For oil-filled cables, the central oil channel can be blocked by the conductor joint, the oil being diverted in the joint envelope. Furthermore, the cable being filled with oil, oil leakages are unavoidable during the work and must be replaced from another entry point to the cable. One can also locally freeze the oil at both sides of the joint with liquid nitrogen. The conductor joint is covered with a metal tube large enough to cover the whole insulation of the cables. The tube is electrically connected to the central conductor, thus providing an electrostatic screen to counter the effect of work imperfections on the local distribution of the electric field at the conductor joint.

The insulation of the joint is reconstituted from two stress cones to uniformly grade the longitudinal field over the distance that the cable sheath is expanded to the joint sheath. A set of metal screens provide uniform grading to the applied voltage within the joint insulation. Their dimensions are determined from the capacitive voltage distribution, a straightforward although tedious process. The insulation around the conductor joint is reconstituted with preimpregnated paper tape, sometimes with the help of a prefabricated insulation sleeve. In general, the insulation of the joint is thicker to reduce the electric field to about half of its nominal value. The electrostatic screen is made of metal tape or carbon and fixed to the insulation. The complete joint is placed in a metallic envelope hermetically welded to the cable sheath. Finally, a protecting envelope completes the cable joint and ensures its mechanical protection.

Terminations: Allow connection between a cable and the phase conductor of an overhead line. The insulation of a cable termination must ensure the transition of the compact cable insulation to that of air atmospheric insulation in overhead line, which requires much larger insulation clearance. The usual way to realize such a transition between the two insulation systems consists of terminating the cable insulation within an insulating housing, generally of porcelain, which provides the required insulation distances for the overhead line. Figure 11.34 illustrates a typical arrangement of an impregnated paper–oil-insulated termination. The cable conductor is joined to a connector, which also blocks the central oil channel. To maintain the dielectric integrity of the cable insulation, the cable sheath is sealed at the base of the porcelain housing, while the electrostatic screen is extended inside along a stress cone constituted from preimpregnated paper tape. A built-up insulation containing potential grading screens follows to ensure an adequate distribution of the applied potential over the exposed portion of the termination insulation.

Wall bushing: Is essentially a back-to-back assembly of two terminations to minimize the dimensions of the passage of a high-voltage conductor through the wall to join two sections of an overhead circuit. It is noticed, in this case, that the potential grading screens occupy the central part of the bushing insulation.

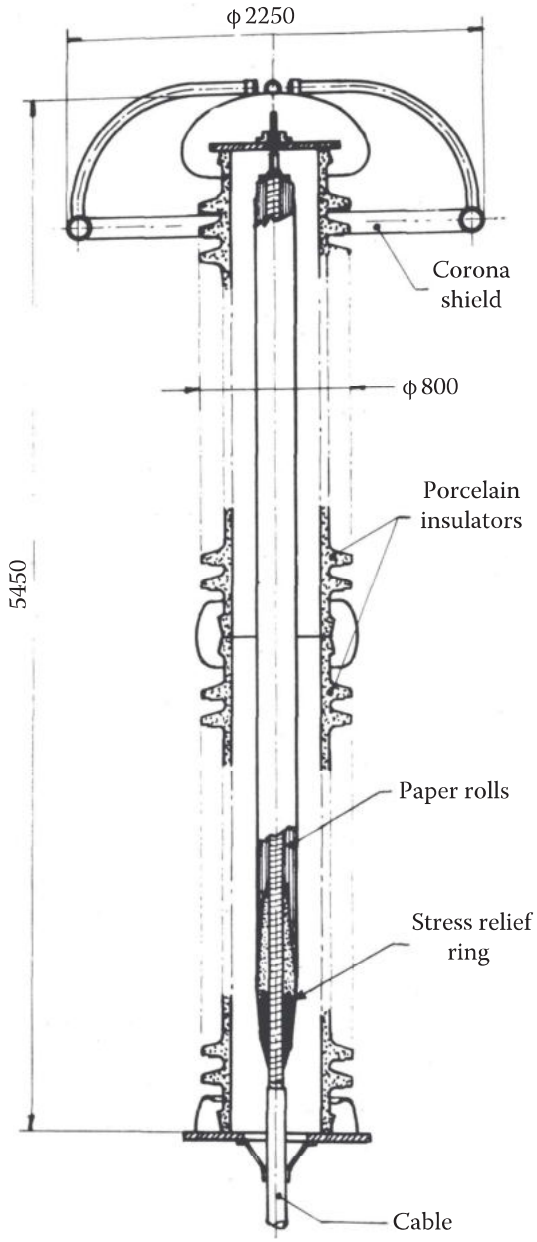

FIGURE 11.34 Illustration of paper–oil-insulated termination. (From Luoni, G. et al., *IEEE Trans. Power Apparatus Syst*., PAS-100(1), 174, 1981.)

11.5.2 Extruded Insulation

The approach described earlier for impregnated paper–oil-insulated accessories applies also to accessories for solid cables with extruded insulation. Figure 11.35 illustrates the general arrangement of accessories. The building of a cable joint follows the same procedure:

- The cable conductors are joined together by compression or welding. Polymer insulation being more sensitive to heat, particular precautions must be taken to limit excessive heating of the cable conductor during the jointing process.
- A conductor shield covers the whole cable insulation to minimize the effect of discontinuity in the dielectric.
- The insulation at the joint is rebuilt, with the same precautions regarding the abrupt change in the insulation thickness at the joint. The insulation is built up along a stress cone to release the stress at the cable shield before it is opened and adequate control of the potential distribution within the joint insulation by means of a set of semiconducting screens.

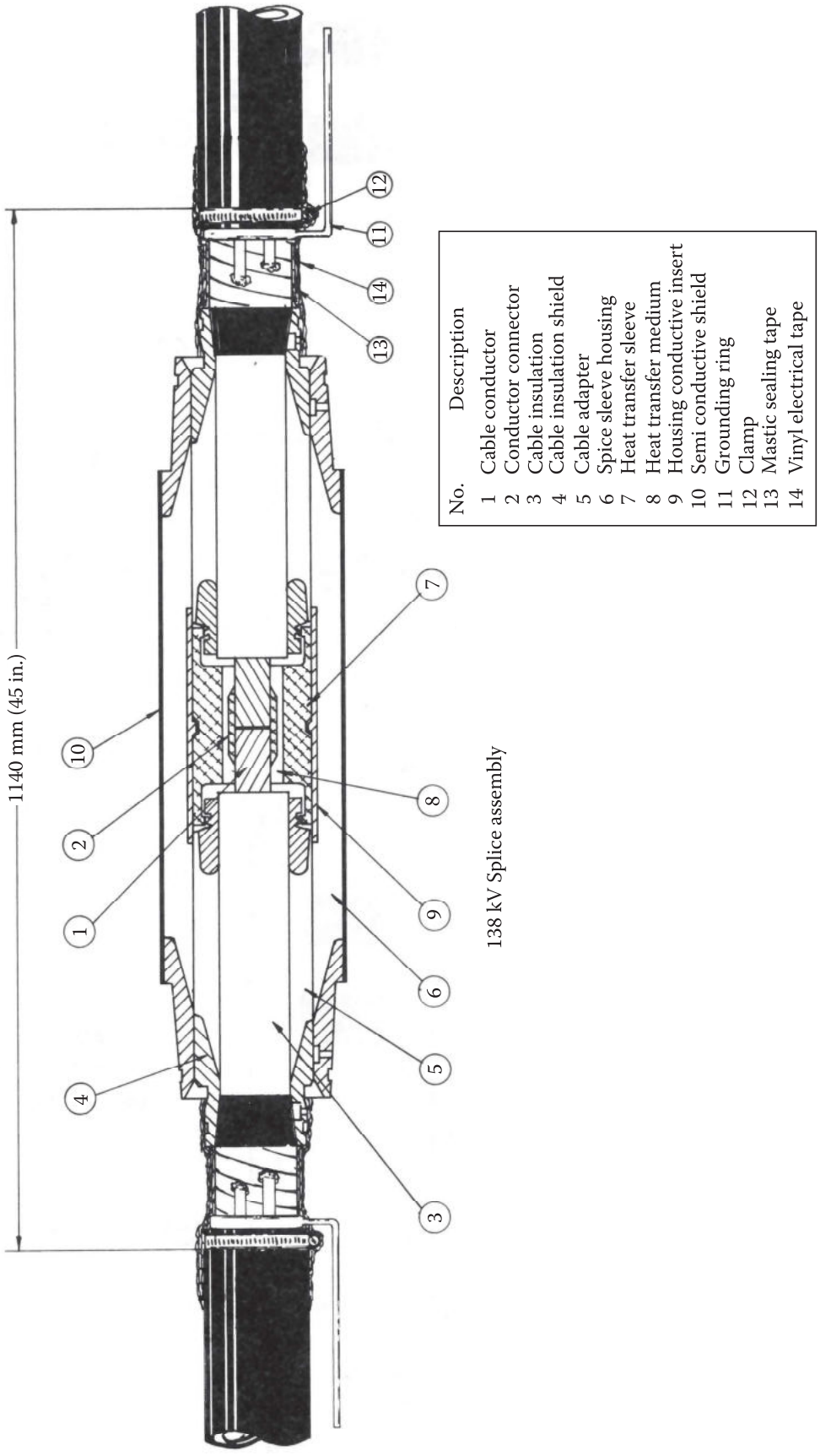

FIGURE 11.35 Illustration of polymer-insulated joints. (From Edgerton, N.W., A premolded splice for 138 kV extruded dielectric cable, *IEEE Trans.*, PAS-97, 2178, 1978.)

- The profile of the stress cone is determined in the same way as for paper–oil-insulated joint. However, the polymer insulation does not favor the installation of multiple semiconducting screens for grading the potential within the insulation, and their number is kept to minimum.

To reconstitute the insulation around the conductor joint, several techniques exist, using copolymerized EPR tape, on-site molding, injection of PE, or using prefabricated insulation. The copolymerized rubber being less dielectrically performing than polymers, its use requires a thicker insulation. This, combined with a high loss factor of the rubber, tends to favor a thermal and electromechanical failure of the joint. However, practical experience shows that the joints with copolymerized rubber tape perform better than certain joints with PE insulation. Such a behavior may be attributed to the high flexibility of rubber to adapt itself to deformations of the conductor during thermal cycles.

The polymer insulation of the joint can be reconstituted by molding. Two techniques have been developed. The first uses PE tape to rebuild the joint insulation. The final insulation is obtained by thermal fusion under pressure to complete the curing of the polymer insulation. This technique provides the reconstituted insulation with a good dielectric withstand under impulse voltage. However, there are still some drawbacks in the long-term behavior of the joints, causing failures subsequent to thermal cycles at full load.

The second technique injects liquid PE in a mold covering the joint and kept under pressure and high temperature to assure the filling of the mold and the adhesion to the cable insulation. The insulation is completed with a semiconducting paint, recovered by semiconducting tape, and secured within a protecting metallic sleeve. The extrusion of polymers being a delicate operation, on-site use of this technique is made only on EHV accessories, 300 kV and higher. For low-voltage cables, prefabricated insulation sleeves of *slip-on* type exist, which simplify considerably their interconnections.

For connection of cables to conductors of an overhead line, impregnated paper–oil-insulated terminations are still used, lacked of fully developed terminations with dry insulation. Figure 11.36 illustrates the typical arrangement of a cable termination. The termination is prepared around a metallic tube replacing the cable conductor. During on-site installation, the cable conductor is pushed in place of the metal tube, and hermetic seals are installed prior to the filling of the termination with oil.

11.5.3 Gas (SF_6) Insulation

With their modular design, gas-insulated cables and equipment do not require specially designed joints. The numerous insulating spacers already required by the modular design are effectively factory-prefabricated joints, which simplify the assembly process while preserving the integrity of the SF_6 insulation.

The connection to an overhead line is provided by gas-insulated terminations of relatively simple design. The SF_6–air interface is ensured by an insulating housing of porcelain or composite resin to provide better protection against the possibility of shattering the porcelain housing subsequent to an internal failure. A gas-barrier spacer is normally used to compartmentalize the equipment from the insulating housing, facilitating its installation. Finally, the field distribution at the surface of insulating housing is controlled by a unique metallic grading screen at ground potential. The adjustment of the length of the grounded grading screen allows a control of the field distribution at the surface of the insulating housing. The arrangement is relatively less effective than grading screens in an impregnated paper–oil-insulated termination. It is often observed that users prefer a paper–oil-insulated termination for gas-insulated cables and equipment, even if this means additional complications related to a second insulation system within the same equipment.

SF_6-insulated terminations exist for use in oil/SF_6 and SF_6/air interfaces and are in service up to voltages of 800 kV ac. Pressurized porcelain housing may shatter following a puncture, with serious consequence to laboratory personnel. IREQ has developed for the needs of the high-voltage laboratory, an SF_6-insulated terminations of 1 MV ac with a BIL of 2100 kV, using a fiber-glass housing, an elegant solution to the problem of shattered porcelain (Figure 11.37). As for gas-insulated wall bushing, it is essentially a back-to-back assembly of two cable terminations to minimize the passage through the wall of a high-voltage connection of two sections of an overhead circuit.

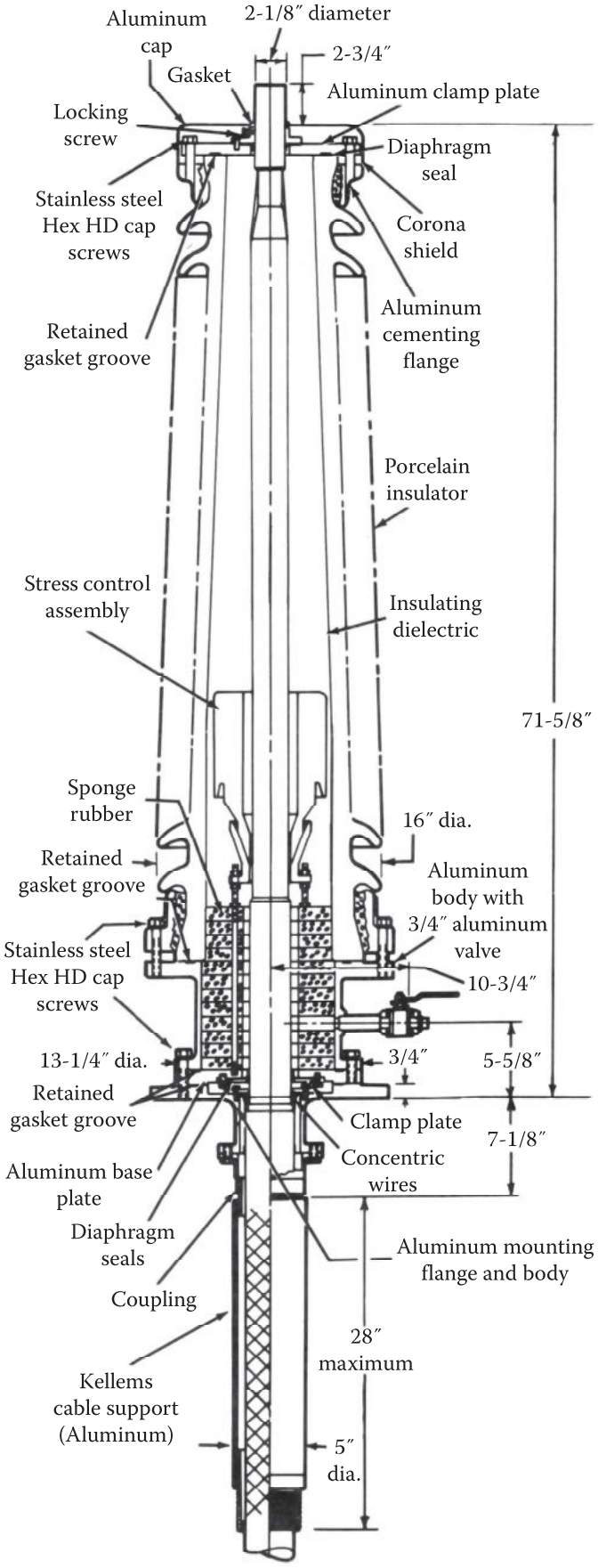

FIGURE 11.36 Illustration of polymer-insulated cable termination. (From Heppner, D.R. and Gear, R.B., New cable terminations for solid cable systems 15 kV and above, *IEEE Trans*., PAS-91, 975, May/June 1972.)

FIGURE 11.37 1 MV ac termination with fiber-glass housing at IREQ. (Photo courtesy of Hydro Québec.)

11.6 High-Voltage DC Cables and Accessories

In general, power transmission by HVDC is less problematic to high-voltage cables. A dc current does not induce circulating currents in the metallic sheath. It does not generate dielectric losses in cable insulation or hysteresis losses in magnetic material. HVDC is also less vulnerable to the development of PDs in voids within cable insulation, allowing a higher operating field as compared with those admissible in HVAC. Field experience has shown that high-voltage cable insulation is more tolerant to dc than ac stress. Furthermore, lower losses associated with dc current allow operating the cables at higher currents, increasing proportionally the power transmission capacity up to 30% higher. Finally, there is no reactive power with HVDC, and hence, the critical length is much longer, limited uniquely by dc voltage drop and resistive losses.

In spite of the numerous advantages associated with HVDC cables, there are only few operating installations, the majority of which concern long-distance submarine system unsuitable for HVAC cables: Kingsnorth, 88 km (53 miles) long, 640 MW at ±266 kV; Gotland, 60 miles long, 20 MW at ±100 kV (upgraded to 150 kV in 1970); and Sardinia, 125 km (75 miles) long. The ±280 kV level was reached in 1969 with the British Columbia to Vancouver Island link (Eyraud et al., 1970), and the level of ± 400 kV with the Finland–Scandinavia link realized in 1989. All use *solid* mass-impregnated cables.

The first application of HVDC-impregnated paper–oil-insulated cables was in 1977 with the British Columbia to Vancouver Island link at ±280 kV and reached the level of ±450 kV in the St. Lawrence River crossing in 1990 (Couderc et al. 1992; Chaaban et al., 1992; Trinh et al., 1992). The use of pipe-type (Allam and McKean, 1981), polymer-, and SF_6-insulated cables for HVDC power transmission is possible although there are still few practical installations to date.

Application of high-voltage cables to the dc power transmission does not require major modifications to the cable design, as long as the various specificities related to this mode of power transmission are taken into consideration. These aspects of the application of high-voltage cables to the HVDC power transmission will be discussed in the following.

11.6.1 Dimensioning of Conductors

The conductors for HVDC cables are simple in design: their structure is standard or of the Conci type (Figure 11.7), since only resistive losses contribute to energy losses. They are proportional to the resistance of the conductor according to (11.14)

The same procedure used for dimensioning of the ac cable conductor still applies for dc cable. The lower losses in dc cables result generally in conductors of smaller size for the same current rating, which often do not require forced cooling.

11.6.2 Dimensioning of the Insulation

For a dc cable, the insulation thickness must take into account the fact that the distribution of the electric field is dictated by volume resistivity of the insulation during the steady-state regime and by capacitive distribution during transient overvoltage.

11.6.2.1 Field Distribution in Steady-State Regime

The volume resistivity of the insulation is a function of both the local temperature and the applied electric field, according to (Fallou, 1965)

$$\rho = \rho_0 \exp(-\alpha\theta)\exp(-kE) \tag{11.37}$$

where

ρ_0 is the resistivity of the insulating material at 0°C
θ is the temperature of the insulating material
ρ is the corresponding value at temperature θ
E is the applied electric field,
α and k are the empirical coefficients of temperature and electric field

Since the dc resistivity of an insulation is a function of both the temperature and field intensity, the exact solution for the dc field distribution is complex. However, an approximate solution for the field distribution in a coaxial cable, taking into account of the variable resistivity of the insulation, Equation 11.38, has been obtained by Eoll (1975) as follows:

$$E(r) = \frac{\delta U_0 (r/r_i)^{\delta-1}}{r_i \left[1-(r_c/r_i)^{\delta}\right]} \tag{11.38}$$

with

$$\gamma = \frac{kU_0}{r_i - r_c}; \quad \beta = \frac{\alpha W \rho_t}{2\pi}; \quad \text{and} \quad \delta = \frac{\beta+1}{\gamma+1}$$

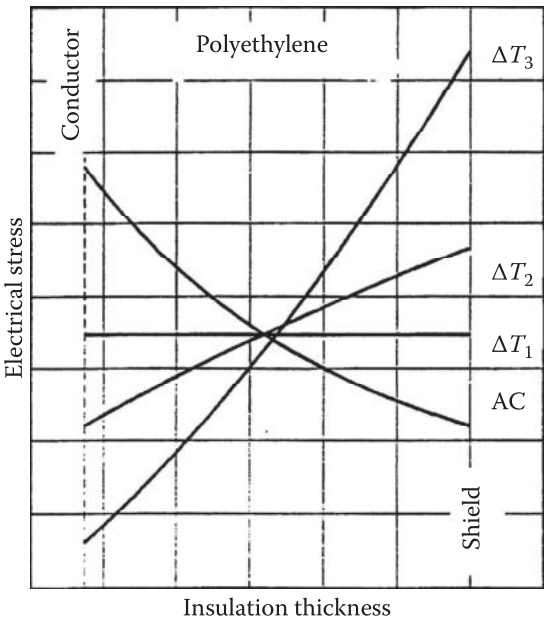

FIGURE 11.38 Distribution of electric field in cable insulation under ac and dc voltages at different loading conditions. (From Khalil, S. *Electr. Insul. Mag.*, 13(6), 35–47, 1997.)

where

$E(r)$ is the field at r in MV/m
r_i is the maximum radius of the insulation in m
r_c is the radius of the conductor in m
W is the resistive losses generated by the conductor calculated according to Equation 11.12 in W/m
U_0 is the applied dc voltage between the conductor and sheath in MV
ρ_t is the thermal resistivity of the insulation in C m/W,
α (C^{-1}) and k (m/MV) are the temperature and field coefficients in Equation 11.38

The distribution of the electric field E between the conductor and the cable sheath varies with the load condition of the cable as illustrated in Figure 11.38, which shows the field distributions in a XLPE cable insulation for different loading conditions (Khalil, 1997). At no load, the field is maximum at the conductor and minimum at the cable shield and is identical to ac field. As the load current increases, the electric field at the conductor is reduced as its temperature rises. At full-load condition, the field may be minimum at the conductor and maximum at the cable sheath.

To take account of this "stress inversion," cable manufacturers sometimes use thin paper tapes not only close to the conductor but also near the cable sheath to reduce the local electric field. However, the peripheral layers of the insulation are more vulnerable than the inner layers in certain conditions (namely, during the bending tests on the cable). It is prudent to limit the design gradient at the cable sheath to a value lower than that at the conductor under conditions of full load, to take account of the inversion of the field within the insulation. The normal practice resides in specifying a maximum temperature difference ΔT between the temperature at the conductor and cable sheath that would result in an acceptable field inversion across the cable insulation.

11.6.2.2 Field Distribution in Transient Conditions

Because of the rapid variations of transient voltages, lightning or switching impulses, the field and potential distribution in cable insulation is controlled by cable capacitance. An important aspect of field distribution in a dc cable is related to its reversal of polarity subsequent to a transient voltage or following a change in the direction of energy transmission. In the latter case, the polarization phenomena being slow, the new charge distribution (of opposite polarity) within the insulation will slowly establish itself after

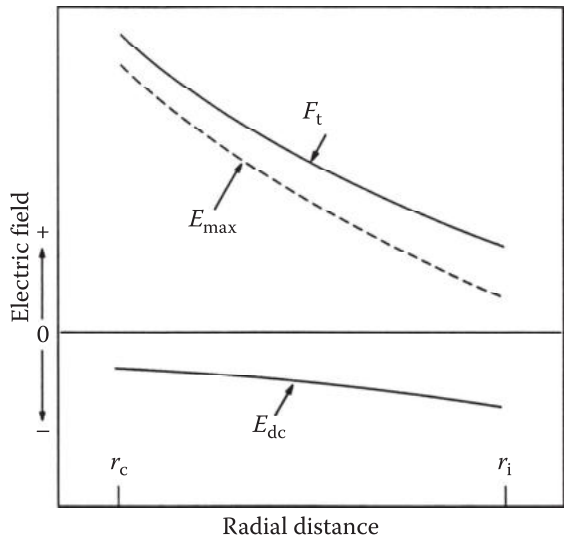

FIGURE 11.39 Distribution of the field under dc voltage superimposed by an impulse voltage of opposite polarity.

polarity reversal of the applied voltage. In transient conditions, the redistribution of charges remains unaffected. As a result, polarity reversal tends to locally overstress the insulation.

Referring to Figure 11.39, it shows the distributions of various stress components within cable insulation when a transient voltage occurs. It can be seen that cable insulation is subjected to a double stress corresponding to the superposition of the transient voltage $v_t(t)$ of amplitude V_t on the applied dc voltage U_{dc}:

$$u(t) = U_{dc} - V_t(t) \tag{11.39}$$

The corresponding electric field $e(t)$ is

$$e(t) = E_{dc} - f_t(t) \tag{11.40}$$

where

E_{dc} is the dc applied field

$f_t(t)$ is the transient field of amplitude F_t

To have a polarity reversal, the amplitude of the transient voltage V_t must exceed the absolute value $|U_0|$ of the applied voltage. The maximum field intensity occurs at the central conductor and has a value of

$$E_{max} = \frac{V_t}{r \ln(r_i/r_c)} - \frac{\delta U_0 (r/r_i)^{\delta-1}}{r_i \left[1 - (r_c/r_i)^{\delta}\right]} \tag{11.41}$$

with δ as defined earlier in (11.38).

11.6.2.3 Field Enhancement in Butt Gap

For ac cables, butt gaps, the free space between two consecutive tapes to facilitate the bending of the cable, are the weak points of the tape insulation. The situation is, however, different for dc cables where the field enhancement is dictated by the resistivities of paper and oil according to

$$\frac{E_h}{E} = \frac{n+1}{1+n\frac{\rho_p}{\rho_h}} \tag{11.42}$$

where ρ_h and ρ_p are the resistivities of the oil and impregnated paper.

For a typical overlay of 70/30, $n = 3$, and the volume resistivities of $\rho_h = 2 \times 10^{13}$ and $\rho_p = 10^{14}$–10^{15}, the field enhancement in the butt gap amounts to less than one, which means that the field in the butt gap is effectively lower than the value for a homogeneous insulation. Thus, in dc, the greater part of the electric field is on the impregnated paper, which has better dielectric strength. This explains also why the impregnated paper–oil cables have better dielectric performance under dc voltage. The breakdown field is 100–120 kV/mm (as compared with approximately 50 kV/mm in ac), which is the same as under impulse voltages, and is practically independent of the rate of rise of the applied voltage (Miranda et al., 1976).

PDs do not significantly affect paper–oil insulation of dc cables as a result of the deposit of charges produced on the wall of the butt gap. The local field within the butt gap is reduced below the onset level of PDs, which are suppressed, and can resume their activities only when the deposit charges are sufficiently neutralized. Aging is much slower under dc voltage. The acceptable maximum gradient within the insulation of paper–oil insulation is 30 kV/mm for nonpressurized mass-impregnated cables and 40 kV/mm for the pressurized cables.

The less severe constraints of dc voltage have allowed the introduction of a new cable design for submarine cable (TOPIST), the structure of which differs considerably from the conventional design (Balog et al., 1987). The lapped insulation is made of bioriented polypropylene tape of 0.025 mm thick, similar to that used in the all-film insulation for condenser. No impregnating fluid is used. The tapes are pressed one upon the other with no possibility for the tape layers to slide during bending of the cable. It is the elasticity of the polypropylene tape that allows the flexion of the cable. The TOPIST cable went through the experimental stage in 1987, having successfully passed the CIGRE bending test (100 m with a radius of curvature of 5 m), the polarity inversion test ($U_0 = 250$ kV), and impulse test (between 1000 and 1100 kV). Aging test was conducted on three lengths of cable to characterize the reliability of the insulating material with encouraging results. The main drawback of this type of cable resides in the very large number of layers required to build up the insulation; the cable must pass three or four times through the taping machine.

Finally, since the electrical conductivity of dc cables is essentially controlled by temperature, the temperature difference across the cable insulation has a pronounced effect on the electric field within the insulation. Forced cooling of the dc cables when applied externally to the cable tends to increase this temperature difference by cooling its external surface and hence to increase the maximum electric field at the cable shield. SCOF cable lends itself easily to forced cooling with the oil channel located within the cable conductor. In practice, one aims at keeping the temperature difference across the insulation in the range of 20°C–25°C.

11.6.3 SF_6-Insulated Cable

In spite of the wide application of gas insulation in ac substation and short links up to the EHV level of 800 kV ac and important research work realized in the field of SF_6 insulation under dc voltage, the feasibility of which has been demonstrated up to the level of ±500 kV, no practical application has yet been made (Cooke et al., 1982; Cookson, 1985). Generally speaking, gas insulation and, by extension, gas-insulated cables and GIS do not have problems with accumulated charges and polarity reversal when operating under dc voltage. However, these problems do exist for the solid insulating spacers. They are of less significant due to the relatively small proportion between solid and gas insulation and to the rather low operating field intensity within the solid dielectric. Charge deposition on the surface of the insulating spacers may occur under conditions of prolonged PDs or repeated flashover at the gas–spacer interface, not expected under normal operating conditions.

Solid particle contamination: Is a specific aspect of gas-insulated equipment. Under dc voltage, the particles, once lift off, cross the whole gas gap and are neutralized at contact with the central conductor and fall back on the envelope, and the process can be repeated again. When the central conductor is at negative polarity, PDs developing at the particles can maintain them in a stationary mode close to the conductor (Cooke et al., 1977; Dale, 1983; Rizk et al., 1979). Such a behavior of particles in a dc electric field tends to indicate that their influence on the dielectric withstand of the gas gap is more critical than under ac.

Figure 11.40 compares breakdown voltage of a coaxial gap under dc and ac voltages under conditions of particle contamination by aluminum wire particles. It can be seen that particle contamination

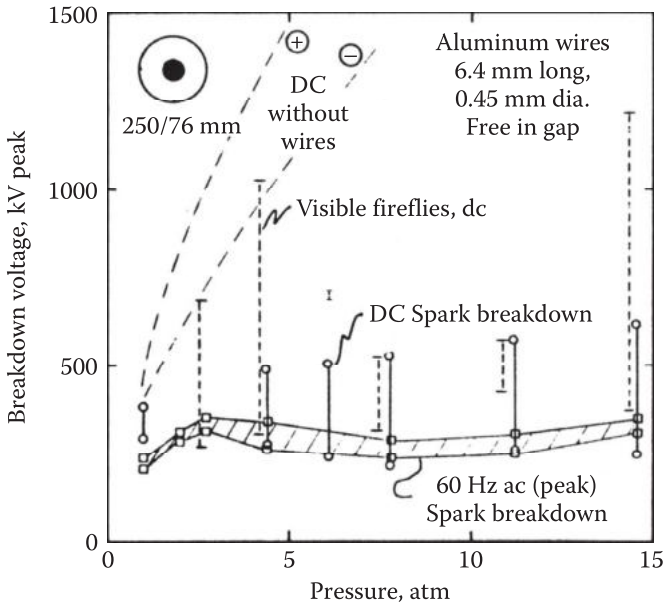

FIGURE 11.40 Effect of particle contamination on breakdown voltage of SF_6-insulated coaxial cable. (From Cooke, C.M. et al., Influence of particles on AC and DC electrical performance of gas-insulated system at extra high voltage, *IEEE Trans., PAS*-96, 768, 1977.)

can significantly reduce the dielectric withstand of the gap, although breakdown voltage with particle contamination does not differ under dc and ac (peak) voltages. Also, the fact that the particles cross the whole gas interval favors their deposit at locations critical to the spacers, that is, close to the central conductor. It is observed that more particles are deposed on the spacers under dc voltage than with ac voltage (Dale, 1983). These considerations on particle contamination may indicate that more precautions may be needed during the installation of gas-insulated cables to minimize the particle contamination.

11.6.4 Accessories

11.6.4.1 Impregnated Paper–Oil Insulation

The design of joint and terminations is similar for dc and ac cables, taking into account the fact that dimensioning of the grading screens is determined by the ratio of the conductivity of the insulating materials. A dc cable joint may be longer (up to ≈40%) than an equivalent ac joint, a direct result of a lower dc design limit field, which is a function of the resistivity of the insulation.

11.6.4.2 Polymer and SF_6 Insulation

No particular change is necessary for the design of accessories for dc voltage application. This is mainly due to the few dc applications of polymer- and SF_6-insulated cables so far. The explanation may simply be the range of dc voltage involved in today's project, between 400 and 600 kV dc, which is too high for polymer-insulated and too low for SF_6-insulated cables.

11.6.4.3 DC Pollution

This problem is dealt with in Chapter 10 on Insulators. As a demonstration of the severity of dc stress and outdoor pollution conditions, we have observed several flashovers on the 500 kV dc cable termination subjected to pollution test at IREQ. The porcelain has a leakage path of 22 m and a height of 6 m. The flashovers take place at voltages of 400 kV dc, with a light contamination (0.02 mg/cm^2) in clean fog. The operating experience of the Itaipu converter station (Brazil) at 600 kV dc shows several in-service failures of the wall bushings, under rain and in presence of a light pollution of the porcelain housing (Rizk and Kamel, 1991). Similar problems occur also in Radisson converter station (Manitoba) at voltages of 450 kV dc. The use of silicon rubber housing or booster sheds appears to offer viable solution to this problem.

11.7 Maintenance Practices Consideration

Being a self-contained system, high-voltage cables do not require any special precaution to operate other than those recommended by the manufacturer to maintain the insulation system at its optimal conditions. However, because of insulation aging, utilities are interested to know the actual state of the insulation and an idea concerning its remaining life.

11.7.1 Actual State of Insulation

Utilities can carry out verifications of the state of cable insulation in view of making decision on the adequacy of the equipment to remain in service via noninvasive measurements of

- The bulk electrical parameters at the terminal points of the equipment, which can be performed on-site
- The aging decomposition by-products, principally dissolved gases in oil, which can be related to the aging state of the individual constituents of the insulation system

Measurement of bulk parameters: Measurement of the PD level and the power-loss factor tanδ remains the principal means to assess the aging state of insulation. The subject is covered in Chapter 14. Monitoring the variations in PD and tanδ with time can give a good appreciation of the aging state of the insulation.

Measurement of the decomposition by-products: Since aging of the insulation produces decomposition by-products of its constituents, the reverse logic implies that the actual state of the insulation system may be assessed from appropriate measurements of their decomposition by-products. This is particularly true for paper–oil insulation where the decomposition by-products are known and well correlated with the aging state of the oil and paper.

Polymers also form decomposition by-products. The small amount of by-products produced and the difficulty to collect them have so far prevented their application in the evaluation of the aging state of polymer, which is evaluated in terms of the density and length of the water and electric trees present in the insulation.

11.7.2 End of Life

End of life represents the final stage of the insulation system, which is then considered as unsuitable for continuing service. However, in practice, the end of life has different meaning for the individual constituent components, paper, oil, etc., and the whole insulation system, which allows the utilities to take appropriate actions in response to specific aging conditions.

Bulk parameters: Measurement of PD and power-loss factor tanδ, although feasible on-site, suffers from a clear definition of end-of-life criteria.

Decomposition by-products: Are currently used to determine end of life of the insulating materials, principally for paper–oil insulation. Their application is, however, limited to criteria for maintenance purposes; the degree of depolymerization gives a good indication of the residual mechanical property of paper. They still suffer from no clear correspondence between the aging state of the materials and the dielectric performance of the insulation as a whole.

Tree length in polymers: The end of life for polymer insulation is more related to the density of water and/or electric trees per unit of length of cable insulation and their dimensions since each one has a probability to develop into breakdown of the insulation. An evaluation of the tree density in the cable insulation near the fault location can be used to determine the length of cable to be replaced. A clear assessment of the end of life remains to be defined in terms of treeing density and length.

REFERENCES

ABB Ltd. SF6 gas-insulated switchgear—Type ELK, 1990.

Allam, E.M. et al. Development and long term testing of a low-loss 765 kV high pressure oil-filled pipe cable. Rapport CIGRE 21-06, Paris, France, 1986.

Allam, E.M. and E.L. McKean. Laboratory development of ±600 kV DC pipe cable system. *IEEE Transactions on Power Apparatus and Systems* PAS-100: 1219–1225, 1981.

Bahder, G., Garrity, T., Sosnowski, M., Eaton, R., and C. Katz. Physical model of electric aging and breakdown of extruded polymeric insulated power cables. *IEEE Transactions on Power Apparatus and Systems* PAS-101: 1379–1390, June 1982.

Balog, G. et al. TOPIST une nouvelle technique de câble sous-marin pour haute tension continue. In: *Conference CIGRE*, pp.122–124, October 1987.

Bellport, B.P. 525 kV cable picked for Grande Coulée. *Electrical World*, pp. 29–31, April 1970.

Boggs, S. and J. Xu. Water treeing—Filled versus unfilled cable insulation. *Electrical Insulation Magazine* 17(1): 23–29, January/February 2001.

Boggs, S.A., Chu, F.Y., Fujimoto, N., Krenicky, A., Plessl, A., and D. Schlicht. Disconnect switch induced transient and trapped charge in gas-insulated substations. *IEEE Transactions on Power Apparatus and Systems* PAS-101: 3593–3602, 1982.

Chaaban, M. et al. Evaluation of HVDC cables for the St-Lawrence river crossing of hydro-Québec 500-kV DC line—Part III: Thermal behavior. *IEEE Transactions of Power Delivery* PWRD-7(2): 609–613, April 1992.

Chu, F.Y. and J.-M. Braun. *Assessment of Moisture in Gas-insulated Substations*. Canadian Electrical Association, report No. 217 T 424, October 1989.

Cooke, C.M., Wootton, R.E., and A. Cookson. Influence of particles on AC and DC electrical performance of gas-insulated system at extra high voltage. *IEEE Trans*. PAS-96, 768–777, 1977.

Cookson A.H. Gas-insulated cables. *IEEE Transactions on Electrical Insulation* EI-20: 859–890, 1985.

Couderc, D. Revue de l'État des Technologies des Câbles de Transport a Très Haute tension en Courant Alternatif et Continu. IREQ Report, November 1987.

Couderc, D. et al. Evaluation of HVDC cables for the St-Lawrence river crossing of hydro-Québec 500-kV DC line—Part I: Dielectric and accelerated aging tests on prototypes. *IEEE Transactions of Power Delivery* PWRD-7(2): 1034–1042, April 1992.

Crine, J.P. Rate theory and polyethylene relaxation. *IEEE Transactions on Electrical Insulation* EI-22(2): 169–174, April 1987.

Cygan, P. and J.R. Laghari. Models for insulation aging under electrical and thermal multistress. *IEEE Transactions on Electrical Insulation* EI-25(5): 923–934, October 1990.

Dakin, T.W. Electrical insulation deterioration treated as a chemical rate phenomena. *Transactions of the American Institute of Electrical Engineers* 67(Part I): 113–122, 1948.

Dakin, T.W. and S.A. Studniarz. The voltage endurance of cast epoxy resins. In: *IEEE International Symposium of Electrical Insulation*, 1978.

Dang, C., Lamarre, L., Landreville, L., Blais, R., and N.G. Trinh. Dielectric Performance of Distribution XLPE-Cable Accessories at High Temperatures. CEA report 139-D-505A, 1990.

Dang, C., Parpal, J.-L., and J.P. Crine. Electrical aging of extruded dielectric cables. Review of existing theories and data. *IEEE Transactions of Dielectrics and Electrical Insulation* DEI-3(2): 237–247, April 1996.

De Maris, S. 500 kV CGI System is installed in the Cascades. *Transmission and Distribution Magazine*, pp. 51, April 1975.

Densley, J. Ageing mechanisms and diagnostics for power cables—An overview. *Electrical Insulation Magazine* 17(1): 14–22, January/February 2001.

Dick, E.P., Fujimoto, N., Ford, G.L., and S. Harvey. Transient ground potential rise in a gas-insulated substation—Problems identification and mitigations. *IEEE Transactions on Power Apparatus and Systems* PAS-101: 3610–3619, 1982.

Edgerton, N.W. A premolded splice for 138 kV extruded dielectric cable. *IEEE Transactions on Power Apparatus and Systems*, PAS-97(6): 2178–2186, November/December 1978.

Eoll, C.K. Theory of stress distribution in insulation of high voltage DC cables—Part I. *IEEE Transactions on Electrical Insulation* EI-10(1): 27–35, 1975.

Eyraud, I. et al. Transport par câbles sous-marins à courant continu à 300 kV entre la Colombie-Britanique et l'Ile de Vancouver. Rapport CIGRE No. 21-07, Paris, France, 1970.

Fallou, M. Nouvelles expériences sur les câbles à courant continu isolés au papier imprégné. *Revue Générale de l'Electricité* 24: 177–190, 1965.

Farnetti, F. et al. Power transmission of a self-contained oil-filled 1100 kV cable system full-scale tests and design criteria. Rapport CIGRE No. 21-09, Paris, France, 1984a.

Farnetti, F. et al. Testing of a 1100 kV, 3 to 9 GVA underground transmission system. *IEEE Transactions on Power Apparatus and Systems* PAS-103: 2034–2042, 1984b.

Fujimoto, N., Dick, E.P., Boggs, S.A., and G.L. Ford. Transient ground potential rise in a gas-insulated substation—Experimental studies. *IEEE Transactions on Power Apparatus and Systems* PAS-101: 3603–3609, 1982.

Fukuda, T. Technological progress in high-voltage XLPE power cables in Japan—Part I. *Electrical Insulation Magazine* 4(5): 9–16, September/October 1988.

Fukuda, T. Technological progress in high-voltage XLPE power cables in Japan—Part II. *Electrical Insulation Magazine* 4(6): 15–20, November/December 1988.

Gazzana Priaroggia, P., Piscioneri, J., and S. Margolin. The long island sound submarine cable interconnection, *IEEE Trans.,* PAS-90(4): 1863–1873, July/August 1971.

Gotoh, H., Okamoto, T., Suzuki, S., and T. Tanaka. Method for estimation of the remaining lifetime of 6.6 kV XLPE cables after their first failure in service. IEEE *Transactions on Power Apparatus and Systems* PAS-103(9): 2428–2434, September 1984.

Graneau, P. *Underground Power Transmission—The Science, Technology and Economics of High Voltage Cables*, Science Publication, John Wiley & Sons, 1976.

Heppner, D.R. and R.B. Gear. New cable terminations for solid cable systems 15 kV and above. *IEEE Transactions on Power Apparatus and Systems*, PAS-91: 975–978, May/June 1972.

Honda, M., Aoyagi, H., Koya, M., Kobayashi, N., and M. Tamura. V-t characteristics of epoxy molded insulation for sustained AC voltage. *IEEE Transactions on Power Apparatus and Systems* PAS-103(5): 1017–1023, May 1984.

Hydro-Québec. Reseau de Transport. April 1978.

Jocteur, R. et al. Développement de liaisons 400 kV isolées au polyéthylène basse densité, Rapport CIGRE No. 21-09, Paris, France, 1986.

Kalkner, W., Miller, U., Peschke, E., Henkel, H.J., and R. vonOlhausen. Water treeing in PE and XLPE insulated High Voltage Cables. *International Conference on Large High Voltage Systems*, CIGRE, paper no. 21-07, 1982.

Khalil, S. International research and development trends and problems of HVDC cables with polymeric insulation. *Electrical Insulation Magazine* 13(6): 35–47, November/December 1997.

King, S.F. and N.A. Halfter. *Underground Power Cables*. London, U.K.: Longman, 1982.

Kobayashi, T. et al. Development of 275-kV internally cooled XLPE cable. *IEEE Transactions on Power Apparatus and Systems* PAS-104(4): 775–784, April 1985.

Kothe, R., Bamji, S., Bulinski, A., and J. Densley. Impulse life tests on field aged XLPE cables containing water trees. In: *IEEE International Symposium on Electrical Insulation*, Washington, DC, June 1986, pp. 37–40.

Kubo, H., Noda, N., Nishino, J., Hata, R., and T. Miyazaki. Development of 275 kV oil-filled cable insulated with polypropylene laminated paper (PPLP). *IEEE Transactions on Power Apparatus and Systems*, PAS-101(12): 4472–4483, December 1982.

Luoni, G., Occhini, C., and B. Parmigiani. Long term tests on a ±600 kV DC cable systems. *IEEE Transactions on Power Apparatus and Systems* PAS-100(1): 174–183, January 1981.

McKean, A.L., Merrell, E.J., and J.A. Moran Jr. EEI manufacturers 500/550 kV cable research project cable C—High pressure oil paper pipe type. *IEEE Transactions on Power Apparatus and Systems*, PAS-90(1): 224–239, January 1971.

Miranda, F.J. et al. Self-contained oil-filled cables—A review of progress. In: *Proceedings of the Institution of Electrical Engineers* 123(3): 229–238, March 1976.

Montanari, G.C., Pattini, P., and L. Simoni. Voltage endurance of XLPE insulated cable modes. In: *IEEE International Symposium on Electrical Insulation*, Montreal, Québec, Canada, 1984, pp. 54–57.

Montsinger, V.M. Loading transformers by temperature. *Transactions of the American Institute of Electrical Engineers* 49: 776–792, 1930.

Moreau, E., Mayoux, C., Laurent, C., and A. Boudet. The structure characteristics of water trees in power cables and laboratory specimens. *IEEE Transactions on Electrical Insulation* EI-28(1): 54–64, January/February 1993.

Nitta, T. and H. Kuwahara. Time dependence of breakdown voltage and endurance testing of compressed gas insulation. *IEEE Transactions on Power Apparatus and Systems* PAS-100(6): 3055–3065, June 1981.

Occhini, E. et al. High voltage transmission systems at 750 and 1100 kV with oil-filled cables—construction and tests, CIGRE 21-08; 1978.

Ogawa, K., Kurata, M., Suzuki, H., Kawasaki, K., and N. Imai. Field test of 275-kV internally water cooled XLPE cable system. *IEEE Transactions of Power Delivery* PWRD-4(1): 8–18, January 1989.

Parpal, J.L., Crine, J.P., and C. Dang. Electrical aging of extruded dielectric cables. A physical model. *IEEE Transactions of Dielectrics and Electrical Insulation* DEI-4(2): 197–209, April 1997.

Rizk, F.A.M., Masetti, C., and R.P. Comsa. Particle-initiated breakdown in SF6 insulated systems under high direct voltage. *IEEE Trans*. 98(3):825–836, May 1979.

Rizk, F.A.M. and Kamel, S.I. Modelling of HVDC wall bushing flashover in nonuniform rain. *IEEE Transactions of Power Delivery* PWRD-6(4): 1650–1662, October 1991.

Sakamoto, Y., Fukagawa, H., Ninomiya, K., Yoshida, S., and N. Ando. Investigation of test method on DC XLPE cable. *IEEE Transactions on Power Apparatus and Systems* PAS-101(6): 1352–1362, June 1982.

Schmidt, W. and V. Szente. Effect of humidity on the electrical strength of SF6 gas-insulated H.V. equipment. In: *IEEE Canadian Conference on Power & Communication*, Montreal, Québec, Canada, 1974, pp. 241–242.

Studniarz, S.A. and T.W. Dakin. The voltage endurance of cast epoxy resins II. In: *IEEE International Symposium of Electrical Insulation*, 1982, pp. 19–26.

Tareev, B.M. *Physics of Dielectric Materials*, Moscow, Russia: MIR Publications, 1975.

Trinh, N.G. Consideration of the effect of a temperature gradient on the dielectric performance of a CGI bus. In: *IEEE International Symposium on Electrical Insulation*, Philadelphia, PA, 1982, pp. 183–186.

Trinh, N.G. et al. Evaluation of HVDC cables for the St-Lawrence river crossing of hydro-Québec 500-kV DC line—Part II: Cable testing facility for dielectric and accelerated aging. *IEEE Transactions of Power Delivery* PWRD-7(2): 1043–1049, April 1992.